Materials Proceedings

MDPI

*Proceedings*

# Properties of Thin Film-Covered GaN(0001) Surfaces †

**Miłosz Grodzicki** [1,2,*]

[1] Institute of Experimental Physics, University of Wrocław, pl. M. Borna 9, 50-204 Wrocław, Poland; Milosz.Grodzicki@uwr.edu.pl

[2] Łukasiewicz Research Network–PORT Polish Center for Technology Development, ul. Stabłowicka 147, 54-066 Wrocław, Poland

† Presented at the 2nd Coatings and Interfaces Web Conference, 15–31 May 2020; Available online: https://ciwc2020.sciforum.net/.

Published: 13 May 2020

**Abstract:** In this paper, the surface properties of bare and film-covered gallium nitride (GaN) of the wurtzite form, (0001) oriented are summarized. Thin films of several elements—manganese, nickel, arsenic and antimony—are formed by the physical vapour deposition method. The results of the bare surfaces as well as the thin film/GaN(0001) phase boundaries presented are characterized by X-ray and ultraviolet photoelectron spectroscopies (XPS, UPS). Basic information about electronic properties of GaN(0001) surfaces are shown. Different behaviours of thin films after post-deposition annealing in ultrahigh vacuum conditions, such as surface alloying, subsurface dissolving and desorbing, are found. The metal films form surface alloys with gallium (NiGa, MnGa), while the semi-metal (As, Sb) layers easily evaporate from the GaN(0001) surface. However, the layer in direct contact with the substrate can react with it modifying the surface properties of GaN(0001).

**Keywords:** GaN(0001); thin films; manganese (Mn); nickel (Ni); arsenic (As); antimony (Sb); alloying; photoelectron spectroscopy

## 1. Introduction

The intensive development of research related to gallium nitride (GaN) arose in the second half of the 1990s. This was due to the improvement in GaN crystals' quality, and their availability on the market, as well as controlling doping techniques, which opened the door for wide use in modern electronic devices [1–3]. The upward trend of research continues to this day, proving the attractiveness of this semiconductor. This stems from the fact that GaN, especially in the wurtzite structure, has many more potential applications in the light-emitter, high-power and high-frequency fields compared to the conventional III-V semiconductors, i.e., GaAs, GaSb [4–10]. This is due to its unique physicochemical properties as a wide and direct band gap along with high electron mobility, thermal conductivity, and breakdown voltage. Furthermore, GaN, due to its high chemical and thermal resistance, enables electronic equipment to operate under harsh conditions, in contrast to electronic devices based on the well-established silicon or germanium semiconductors. The high popularity of GaN-based materials is also due to the easy method of band structure tuning by substituting one of elements for another from the same atomic group, creating a new III-N alloy of the wurtzite form [8,10]. An operation of the GaN-based device depends on the quality of heterostructures, which in turn is subject to the starting GaN surface. The (0001) surface terminated with gallium atoms is the most commonly used form of GaN in the electronics industry, and therefore it is important to get a deep insight into properties of the GaN(0001) surfaces. In turn, the properties of thin-film systems, especially the metallic films deposited on semiconductors, are also extremely important because they are basic and necessary parts of all electronic structures. The

simple device, i.e., contact, plays a crucial role in the functionality of electronic components and may show a different electrical behaviour. It can have the Ohmic or Schottky characteristic. However, both these types are extremely substantial for electronics. The contact behaviour for the GaN-based electronic device is determined by the properties of the thin film/GaN phase boundary, which depends on the properties of the bare GaN(0001) surface itself and the characteristics of the deposited material. Manganese (Mn), nickel (Ni), are present in many electronic devices [9]. It was found that Mn is a very attractive material for creating a ferromagnetic MnGaN semiconductor by molecular beam epitaxy (MBE) [11,12] and therefore for creating hybrid systems with spintronic potential [13,14]. Mn on GaN was studied using the scanning tunnelling microscopy (STM) technique [15–19] as well as by photoemission experiments [20–24]. Thin films of Ni on GaN were studied in the works [25–31]. This chemical element is a candidate for contacts with GaN. The electric contacts using Pd/Ni bilayers improve device performance [32]. The interfacial reaction between nickel and GaN can occur during annealing [33], which is a commonly used step for contact creation. This can lead to the formation of new Ni-Ga alloys, similarly to the case of the Pd/GaN interface [34], that have catalytic potential [35–41]. In addition to metals, another interesting group of materials deposited as thin layers on GaN surfaces are semi-metals, such as arsenic (As) and antimony (Sb). Processes of MBE growth with As [42–45] and antimony Sb [46,47] as surfactants were performed to increase the quality of GaN films. Furthermore, As incorporated into GaN changes the electronic properties of the host [48–51]. Antimony was also used to modify the properties of GaN [52–54] and to form GaNSb films with p-type character [55,56]. The interaction of As and Sb with GaN, as well as the morphological changes caused by post-deposition annealing, were studied in Refs. [57,58], where it was shown that thermal treatment leads to easy desorption of the films, but some adsorbated atoms remain on the surface modifying its properties.

The basic studies of the interface between GaN and thin layers attracts a lot of attention in both the fundamental and application research. However, in order to interpret them correctly, it is necessary to understand the differences of electronic structure of bare *n*-, *p*- and non-doped GaN (0001) surfaces. Despite the very rich availability of professional literature in these topics, and very good extensive review works [59–61], there are still papers containing misinterpretations of the basic results obtained in photoemission experiments. This is, among other things, due to: (i) the relatively difficult cleaning procedure of the GaN surface, which may lead to changes in its stoichiometry. The bare and metal-covered surface can easily be enriched with gallium [29,34,62], which can lead to a bad interpretation of the deconvoluted Ga-3d components; (ii) the presence of a large number of Ga Auger lines which may overlap others' core level spectra; and (iii) surface photovoltage (SPV) effects which can cause changes in the Fermi level position versus the valence band maximum [63,64]. Furthermore, SVP can sometimes even lead to the appearance of a quasar Fermi level in the metal/GaN system [30], which can be mistakenly interpreted as a chemical shift.

Herein, the differences between photoelectron spectra of bare GaN(0001) achieved by three various X-ray sources, i.e., non-monochromatic Mg $K_\alpha$ (1253.6 eV), non- and monochromatic Al $K_\alpha$ (1486.7 eV) are presented. Such information shows differences in spectra and is particularly useful for materials research, where the correct interpretation of the results can be problematic. This article also presents a review of the author's studies on thin films on the GaN(0001) surface including the metals (Mn, Ni) and the semi-metals (As, Sb). Furthermore, this paper shows three scenarios of thin film behaviour under the influence of annealing in ultrahigh vacuum (UHV) conditions: (i) surface alloying for the Ni, Mn metals; (ii) dissolving in subsurface layers of the substrate in reference to Mn; (iii) and desorbing in the case of the As, Sb semi-metals. The results show that the electronic properties of the GaN(0001) surface obtained after evaporation of thin-films are modified by dissolution or by presence of reacted adsorbate layer.

## 2. Method

All results presented in this paper were obtained on samples of non-doped, *n*- and *p*-type wurtzite GaN(0001) epilayers which had been grown using metal-organic vapour phase epitaxy (MOVPE). Most thin films were deposited in a standard UHV chamber using the physical vapour

deposition (PVD) method with one exception of arsenic which were also deposited by PVD but in an MBE chamber interconnected with an analytic system. The formation of thin film systems as well as measurement were done in situ at room temperature (RT). The physicochemical properties of the bare and thin film-covered GaN(0001) surfaces are obtained by means of X-ray photoelectron spectroscopy (XPS) using non-monochromatic 1253.6 eV or non- and monochromatic 1486.7 eV photons. The electronic properties were measured using ultraviolet photoelectron spectroscopy (UPS) with a non-monochromatic excitation source of 21.2 eV. Photoelectrons were collected by a hemispherical electron energy working in a constant analyser energy mode (CAE) with a step size of 0.05 eV or 0.1 eV and a pass energy of 20 eV in case of XPS measurements. A step size of 0.025 eV and a pass energy of 2 eV were applied for UPS experiments. All binding energies (BEs) were referred to the Fermi level ($E_F$), the position of which was determined using an Ar-ion cleaned reference Ag sample. No charge effect of samples was observed, thus no BE corrections were performed for the presented data. Structural analysis presented herein was carried out using the low-energy electron diffraction (LEED) technique.

## 3. Results and Discussion

### *3.1. Bare GaN(0001) Surface*

The GaN material contains gallium and nitrogen atoms in 1:1 stoichiometry forming the hexagonal N-Ga diatomic layer in which the atoms are arranged in an imperfect tetrahedral geometry due to different atom sizes and electronegativity of Ga and N atoms. The hexagonal N-Ga diatomic layers forming hcp structure can be stacked on top of each other in *c*-direction taking places A, B or C, as shown in Figure 1. There are two stable GaN structures with the ABAB ... or ABCABC ... stacking sequences, for which GaN crystals are obtained in the form of the wurtzite or the zinc-blend, respectively. In addition to being different in structure, both materials have other electronic properties [65–68]. The GaN(0001) has the wurtzite form and is terminated with Ga atoms, unlike to the (000$\bar{1}$) surface on top of which N atoms are situated.

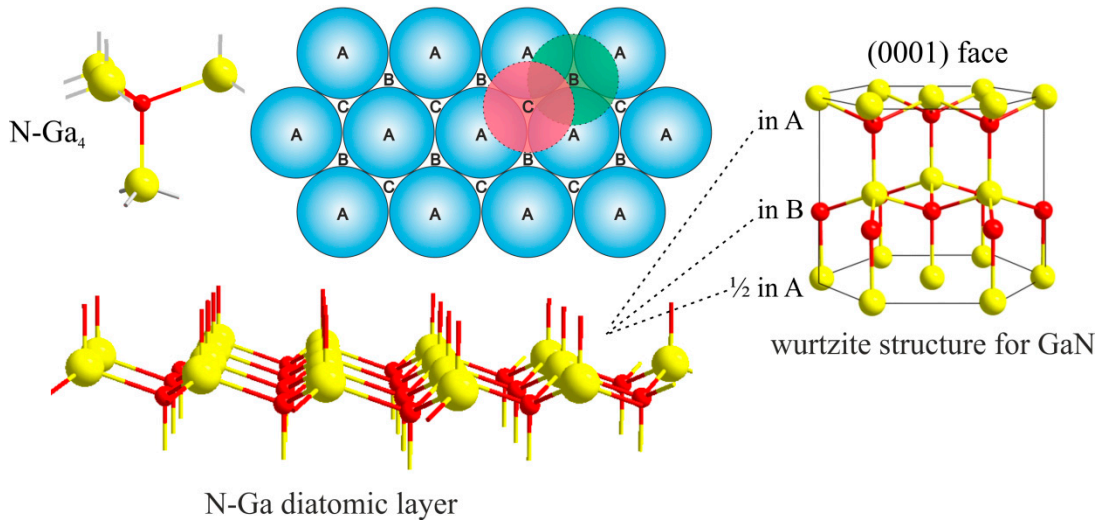


**Figure 1.** Structure of gallium nitride (GaN): particle of $Ga_4N$ in tetrahedral geometry, N-Ga diatomic hexagonal sheet, hexagonal close-packing (hcp) position model, and hcp structure with layering ABAB type.

Below are the results of the non-doped GaN, (0001)-oriented sample, pre-cleaned with isopropanol then cleaned in situ using one short-time annealing under UHV conditions at a temperature of about 800 °C. The broad XPS spectra of the sample obtained with 1253.6 and 1486.7 eV photons are shown in Figure 1. Besides the Ga-2p, Ga-3s, Ga-3p, N-1s peaks from GaN, the C-1s, O-1s core-level lines that are derived from carbon and oxygen impurities are also visible. Auger electrons emitted from a sample exposed to X-rays also contribute to the collected spectra. They

form characteristic energy levels from Auger transitions in atoms presented on surfaces and subsurface layers. In Figure 2, there are many electrons from Ga LLM transitions, and especially two intensive levels, i.e., the $L_3M_{45}M_{45}$ and $L_2M_{45}M_{45}$, with kinetic energies of about 1065 and 1091 eV, respectively. It is also worth noting that the kinetic energy of Auger electrons does not depend on the energy of excitation radiation (unlike photoelectrons). Thus, the same Auger levels in spectra obtained with different photon energies are located at different places of BE, as shown in Figure 2. Furthermore, in the case of measurements with Mg $K_\alpha$ excitation line, a carbon content on GaN surfaces cannot be determined because the C-1s line is covered by one of the Ga LMM levels. For experiments with Al $K_\alpha$ photons, the N-1s line partly overlaps with the Auger signal.

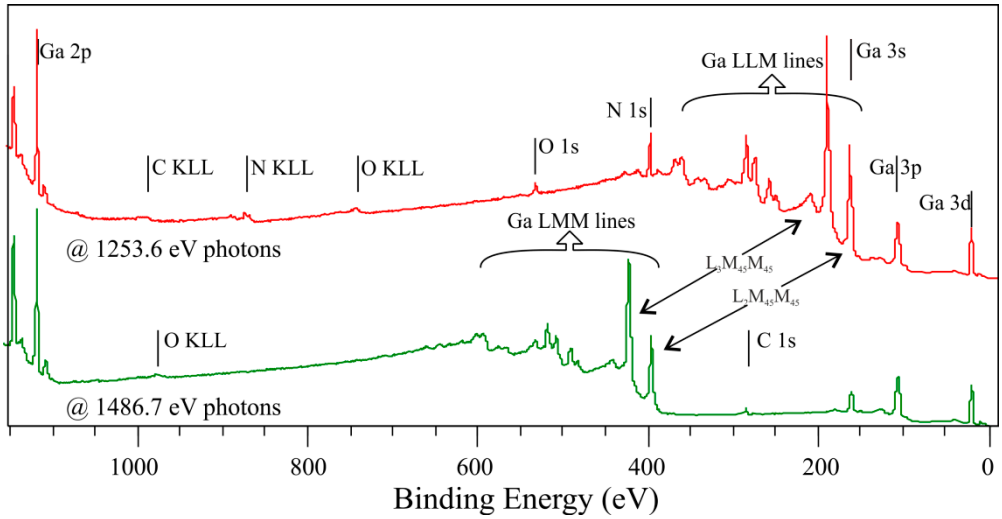


**Figure 2.** Survey spectra for non-doped GaN(0001) surface collected with different photon energies.

The influence of standard commonly used radiation sources on the obtained spectra shape is shown in Figure 3. On the GaN(0001) surface, where a trace amount of oxygen is presented, the Ga-3d shallow core-level line with a BE of 20.4 V contains four sub-peaks. The main one is from the Ga-N bonds, while the two others correspond to Ga-O and Ga-Ga bonds, and the last one comes from the overlap N-2s state [22,51,69]. The X-ray source type has little effect on the shape of Ga-3d peaks obtained, but this is not the case for the valence band (VB), where the impact is significant, as shown in Figure 3a. This is due to the overlap of the X-ray satellite of the Ga-3d on the VB measured with non-monochromatic sources and the different depths from which the electrons originate. The kinetic energy of ejected electrons from the VB excited with 1253.6 eV (Mg $K_\alpha$) and 1486.7 eV (Al $K_\alpha$) photons varies significantly, causing them to have different inelastic mean free paths. This results in signals collected with different photon sources coming from various sample depths.

Despite different shapes, the valence band maximum (VBM) is located 2.7 eV below the $E_F$, found from a linear extrapolation of the leading edge of the spectrum to the background. In Figure 3b, the N-1s spectrum collected with Mg $K_\alpha$ photons consists of two elements: the first is assigned to the N-Ga bonding with the BE of 397.8 eV, and the second to N–H bonds. This spectrum obtained with Al $K_\alpha$ excitation line has five sub-peaks: similarly, the first two peaks corresponding to the N-Ga and N-H bonds and the others coming from the Ga LMM. The Auger signal is suppressed for measurements with a monochromator. The energy difference between the N-1s and Ga-3d peaks is $\Delta E_{\mathrm{N-Ga}}^{\mathrm{GaN}} = \mathrm{BE(N1s)} - \mathrm{BE(Ga3d)} = 377.4$ eV and is consistent with the other literature for GaN [63].

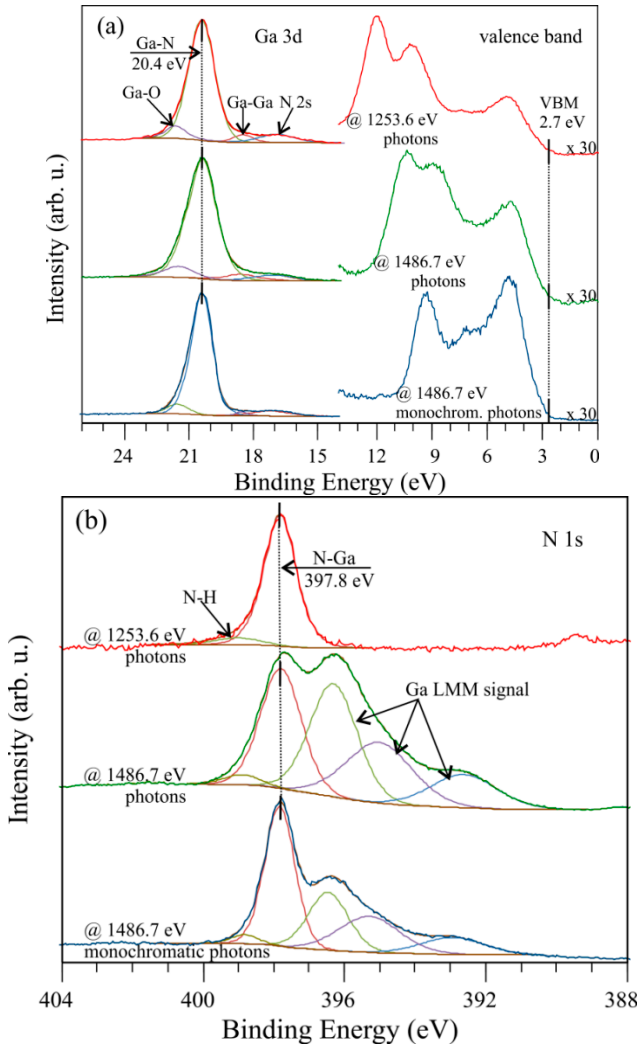


**Figure 3.** X-ray photoelectron spectroscopy (XPS) spectra of (**a**) the Ga 3d and valence band as well as (**b**) the N 1s for the non-doped GaN(0001) surface collected with different photon sources.

Cleaning the surface of GaN crystals under UHV is problematic because it can lead to changes in the surface stoichiometry, regardless of whether it is an ion bombardment or annealing. Ion bombardments may introduce defects and preferentially remove nitrogen atoms [62,70,71]. To eliminate this effect, the post-bombardment annealing method or low-energy N-ion bombardment can be utilized [72–74]. The most convenient and simplest technique of surface preparation in UHV is annealing. However, during this process, the surface may also be decomposed [75]. Thus, rapid thermal annealing (RTA) should be applied. The effect of carbon and oxygen contaminants elimination by this method is shown in Figure 4. One can see that annealing in UHV may lead to achieving the carbon- and oxygen-free GaN(0001) surface. Unfortunately, sometimes this method does not cause complete elimination of contaminants, of which XPS signals remain on the level as the middle curves in Figure 4. This is most likely dependent on the results of pre-cleaning the sample surface by chemical treatment prior to placing it in UHV systems.

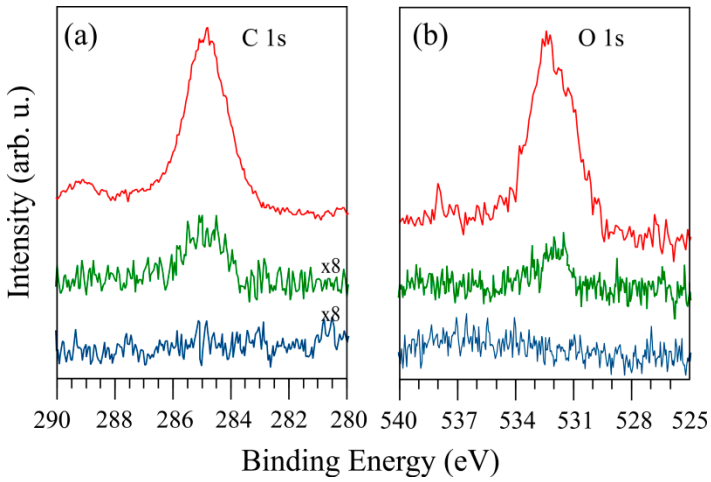


**Figure 4.** XPS spectrum intensity of (**a**) the C 1s and (**b**) the O 1s for non-doped GaN(0001) surface. Upper spectrum corresponds to the degassed surfaces in UHV, lower ones show influence of different number of annealing cycles at 800 °C.

RTA can also guarantee obtaining a high-quality surface, as confirmed by LEED patterns in Figure 5a, where the strong intensity and sharp spots of GaN(0001)-(1 × 1) are visible. Several cycles of RTA may rebuild the surface, forming a facet-like terrace structure changing the diffraction pattern [76,77]. As a result of such rebuilding, the sextets of diffraction spots appeared in hexagonal configuration around each main spot (see Figure 5b). The energy positions of core level line measured by XPS may vary significantly depending on the type and concentration of the dopant used in GaN. Those peak shifts do not necessarily result from the chemical properties of the surface, but may only arise from different locations of the Fermi level in *n*-, *p*- and non-doped GaN. In the perfect, non-doped GaN, the $E_F$ in bulk falls more or less in the middle of the forbidden gap, in the *n*-type it is located close to the conduction band minimum and in the *p*-type it is placed near the valance band maximum. Since photoemissions are surface-sensitive techniques, the $E_F$ position on the surface of the tested material is crucial. Due to the surface density of states present on the GaN(0001), the surface Fermi level is located in a different location than in bulk [64,78–80]. This means that the energy bands at the surface are bent upwards or downwards depending on the dopant type. Figure 6 shows the distance between the valence band maximum and the surface Fermi level for Si- (*n*-), Mg- (*p*-) and non-doped GaN.

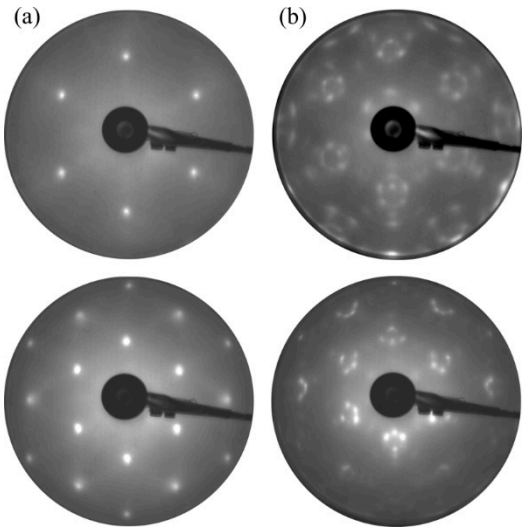


**Figure 5.** Low-energy electron diffraction (LEED) patterns for GaN(0001)-(1 × 1) structure. Image (**a**) is attributed to flat well-ordered surfaces, (**b**) shows the presence of facets. Images are taken with electron beam of 90 (upper) and 155 eV (bottom).

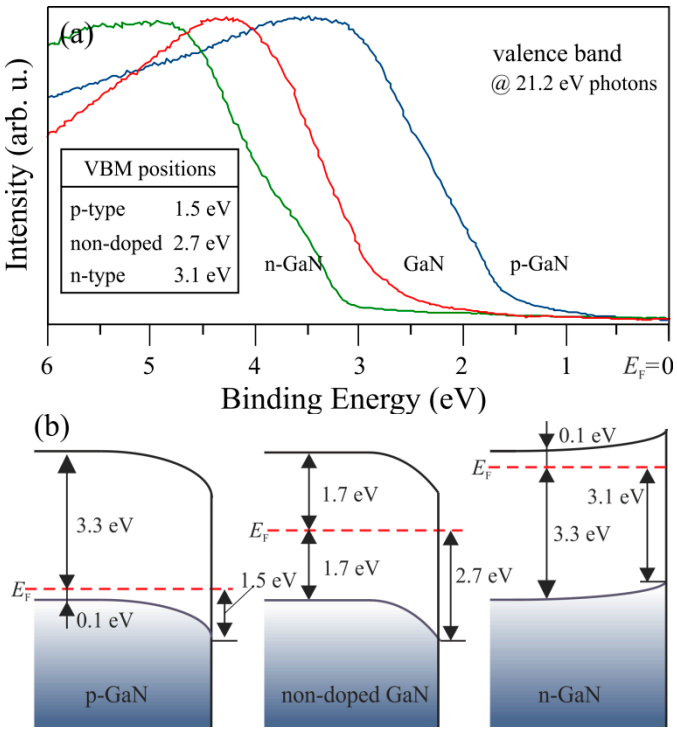


**Figure 6.** (**a**) Ultraviolet photoelectron spectroscopy (UPS) spectra of valence band for *n*-, *p*- and non-doped GaN(0001). (**b**) Energy band diagrams visualisation of (**a**). The Fermi level positions in bulk materials were determined for n- and *p*-type GaN with the carrier concentration of $5 \times 10^{16}$ and $5 \times 10^{17}$ cm$^{-3}$, respectively.

Furthermore, it indicates the difference in the $E_F$ location on the surface and bulk. Moreover, SPV appears on GaN during XPS and UPS measurements, as a result of which the band bending changes [63,64]. Thus, the surface $E_F$ position relative to the VBM may also vary depending on the magnitude of the SPV. Therefore, to determine whether the peak shift is caused by chemical reaction or not, its location relatively to the VMB needs to be known. For instance, on the well-prepared GaN(0001) surface, the Ga-3d state is located around 17.7 eV above the VBM. For the non-doped GaN $\Delta E_V$ = Ga-3d – VBM = 17.7 eV, as seen in the results shown in Figure 3a. There are also different values of the $\Delta E$ in the literature with a spread of ± 0.3 eV from that indicated here.

### *3.2. Mn on GaN(0001)*

Manganese belongs to the transition metals, in group VII in the periodic table. The element exhibits poor electrical and thermal conductivity properties. Manganese has a density of 7.2 g/cm$^3$, its thermal conductivity is 7 W/(m·°C) and its electrical resistivity amounts to $1.6 \times 10^{-6}$ Ω·m (at RT). It melts at 1246 °C and its boiling point is 2061 °C (under standard pressure). Mn needs a high temperature to be evaporated in a vacuum and at 930 °C has a vapour pressure of $10^{-8}$ mbar. Manganese has a multifaceted field of industrial uses, from metallurgy, particularly in stainless steels, to electronic applications.

Surface techniques were used to measure the interfacial behaviour of Mn and GaN in the context of the possible formation of diluted magnetic semiconductor layers. The studies were inspired by spintronic potential of MnGaN alloys [12–14]. Thin films of Mn on GaN have mainly been reported for the $(000\bar{1})$, N-terminated, surfaces [18–20,81–83]. These works, generally, referred to structural analysis for ultra-thin coverages. One exception of this is Ref. [20], where the interaction of Mn with GaN$(000\bar{1})$ was investigated by photoemission experiments with a synchrotron radiation. The results of Mn thin films on the GaN(0001) surfaces concerning structural characterization by STM were reported in Refs. [15–17], whereas the physicochemical properties of Mn on GaN(0001) were studied by the author using XPS and UPS with non-monochromatic excitation sources in works [22–24].

Early stages of coating the non-doped GaN(0001) surface with Mn films and the influence of annealing on the system properties were described in Ref. [22,23]. The growth of Mn film by PVD and characterisation were performed in situ on MOCVD GaN(0001). The initial bare surface that was prepared by RTA exhibited the (1 × 1) structure (confirmed by LEED similar to that in Figure 5a) and had a trace amount of oxygen. In these works, the Mn films formed at RT gave no diffraction patterns, indicating that they are amorphous. The changes in the Ga-3d, N-1s and Mn-2p core level lines with thickness of deposited Mn film are shown in Figure 7. The peaks of the bare surface contained the same components as already presented in Figure 3. Namely, the sub-peaks for the Ga-3d are from the Ga-N, Ga-O, Ga-Ga bonding and the N-2s state. The sub-peaks for the N-1s origin from the N-Ga, N-H bonds. One can see that the substrate XPS lines shift towards a lower BE after deposition of Mn films. The Mn-3p peak behaves in the same manner.

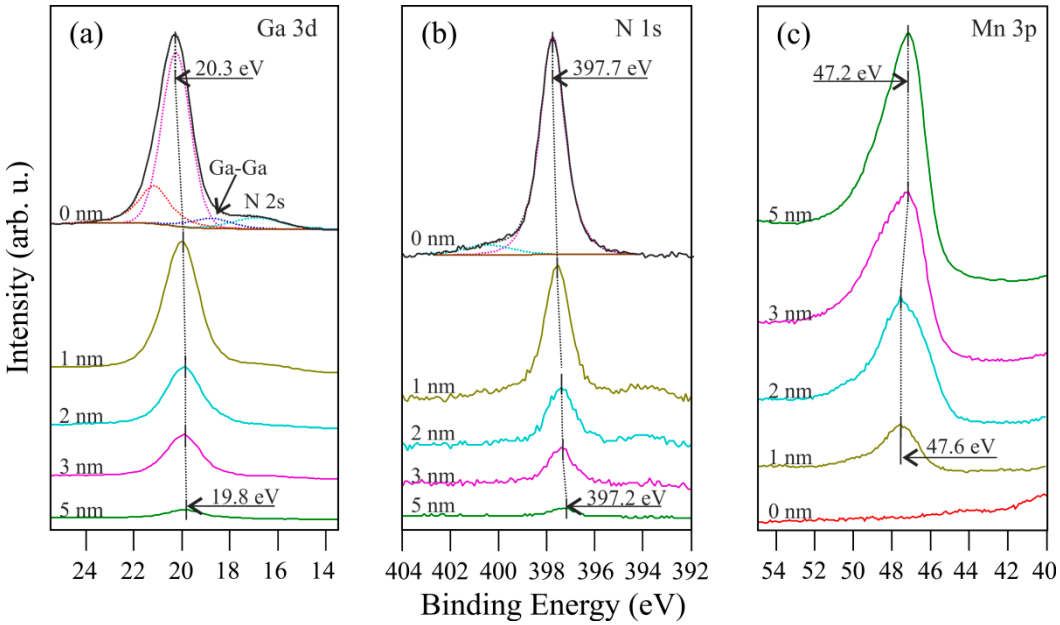


**Figure 7.** Evolution of spectra for (**a**) Ga-3d, (**b**) N-1s and (**c**) Mn-3p with the thickness of deposited Mn film. XPS measurements were performed with non-monochromatic 1253.6 eV photons. Data previously published in [22].

The peak shifts are a result of charge transfer through the Mn/GaN phase boundary and not a chemical reaction of Mn with the GaN. Mn films behave unlike those deposited on the (000-1) surface [20]. The electron transfer at the interface causes the formation of the Schottky barrier, the height of which (SBH) can be simply calculated from the formula: $\mathrm{SBH}_{\mathrm{GaN}}^{\mathrm{Mn}} = \mathrm{E_g} - \mathrm{VBM}_{\mathrm{GaN}}^{\mathrm{Mn}}$, where $\mathrm{E_g}$ = 3.4 eV is the band gap of the GaN, and $\mathrm{VBM}_{\mathrm{GaN}}^{\mathrm{Mn}}$ is the position of VBM at the interface after Mn deposition. The latter value cannot be obtained directly from UPS measurements since the GaN is coated with the Mn, which introduces a new electron density of states (DOS). This means that the VB of the GaN is no longer visible, as presented in Figure 8. However, the VBM for the thin film-covered GaN can be determined indirectly from the Ga-3d peak shift due to the energy distance between the Ga-3d and the VBM is constant $\mathrm{Ga3d_{GaN}} - \mathrm{VBM_{GaN}} = \mathrm{Ga3d}_{\mathrm{GaN}}^{\mathrm{Mn}} - \mathrm{VBM}_{\mathrm{GaN}}^{\mathrm{Mn}}$. This procedure was previously applied to metal films on SiC [84,85]. In Figure 9, the energy level diagrams of the bare GaN(0001) and Mn/GaN(0001) interface with the SBH is constructed based on the UPS and XPS data.

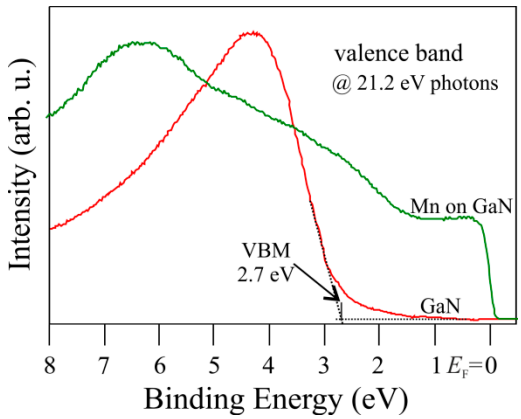


**Figure 8.** UPS spectra of valence band for bare and Mn thin-covered GaN(0001) surface.

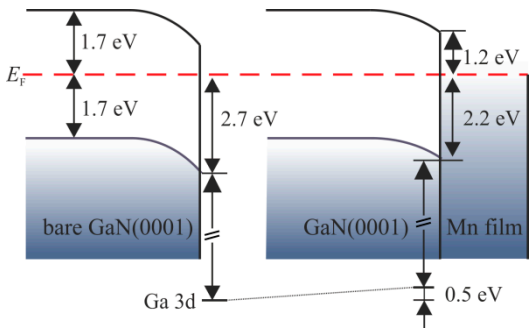


**Figure 9.** Energy band diagrams for bare and Mn film-covered GaN(0001) surface. As seen SBH can be simply calculated based on photoelectron spectroscopy measurements.

Annealing of the Mn films on GaN(0001) in UHV is interesting from the aspect of the Mn-diluted GaN semiconductor formation. The dissolution of Mn atoms in bulk GaN(000-1) induced by thermal treatment was observed using STM [18] and secondary ion mass spectrometry (SIMS) [86]. (Mn)GaN films obtained that way show ferromagnetic behaviour [87]. Experiments examining the changes in physicochemical properties of the films on the GaN(0001) crystals under the influence of annealing were presented in the author's works [23,24]. In Ref. [23] the Mn film-covered non-doped GaN(0001) was annealed at 500 °C followed by 800 °C for 3 min for each temperature. The process strongly modified the morphology of the system. The Mn films on GaN(0001), which are amorphous as grown, crystallize following annealing at 500 °C. LEED patterns for this stage reveal diffraction rings, as shown in Figure 10a. They come from randomly oriented rotational domains of (2.3 × 2.3) structure in relation to the substrate, giving the lattice parameter equal to 7.3 Å. This value matches the $\alpha$-Mn(111), for which the surface lattice constant is from 7.39 to 7.68 Å [88]. The small transformation of the lattice can be attributed to Ga incorporation into the Mn structure. After annealing at 800 °C, the thin film alters into the well-ordered MnGa surface alloy. The LEED pattern, in Figure 10b, exhibits three sets of (1.21 × 1.21)squareR15 structures coming from the film with lattice constant equal to 3.86 Å. They are rotated at 60° relative to each other. The achieved lattice parameter is in line with the structure of the single-phase $Mn_{1+x}Ga$ ($0 < x < 1$) alloys for which the lattice constant is around 3.88 Å [89], clearly demonstrating the formation of alloys on the surface.

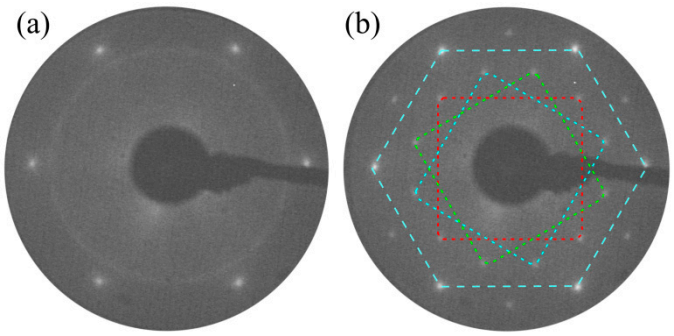


**Figure 10.** LEED patterns (55 eV) for the Mn film-covered GaN(0001) after annealing at (**a**) 500 and (**b**) 800 °C. The three domains of the square structure of MnGa alloy and (1 × 1) hexagonal structure of GaN(0001) substrate are marked. Data previously published in [23].

XPS and UPS provide information on the physicochemical properties of the annealed system. The changes in the Mn-2p doublet introduced by thermal treatment are presented in Figure 11a. The analysis of the Mn-2p$_{3/2}$ peak for the non-annealed system shows that it can be fitted by two sub-peaks with BEs of 368.7 and 639.75 eV. Annealing means that the Mn-2$_{3/2}$ becomes broader, and to reproduce its shape, other components need to be added with BEs of 641 and 642.85 eV. Figure 11b shows that the Ga-2p$_{3/2}$ peak can be fitted by one or two sub-peaks for the non- and annealed system, respectively. They are located at 1117.6 and 1116.5 eV. The sub-peak at a lower BE in the case of the bare GaN(0001) surface corresponds more or less to the Ga-Ga bonding but on the annealed Mn-covered GaN surface should be attributed to the Mn-Ga bond, which has a metallic character with a very weak chemical shift [90]. The sub-peak intensities for both the Mn-2p$_{3/2}$ and Ga-2p$_{3/2}$ states depend on annealing temperature. The changes to both the core level lines, appearing during annealing, are the result of atoms exchange at the phase boundary. There are two processes, i.e., some manganese atoms diffuse into the substrate substituting gallium elements at a subsurface region. In turn, these release Ga atoms directly to the Mn film covered surface. These processes result in the formation of: (i) the (Mn)GaN-like alloy, which is demonstrated by the two extra sub-peaks in Figure 11a (curve 2 and 3 from the top) [21,91], and was already reported in other works [18,86]; and (ii) the Mn-Ga surface alloy, manifested by the second component in Figure 11b (curve 2 and 3). This surface alloying—the intermixing of Ga atoms with thin film on the GaN(0001) surface—is also observed in the case of Ni and Pd adsorbates [29,34].

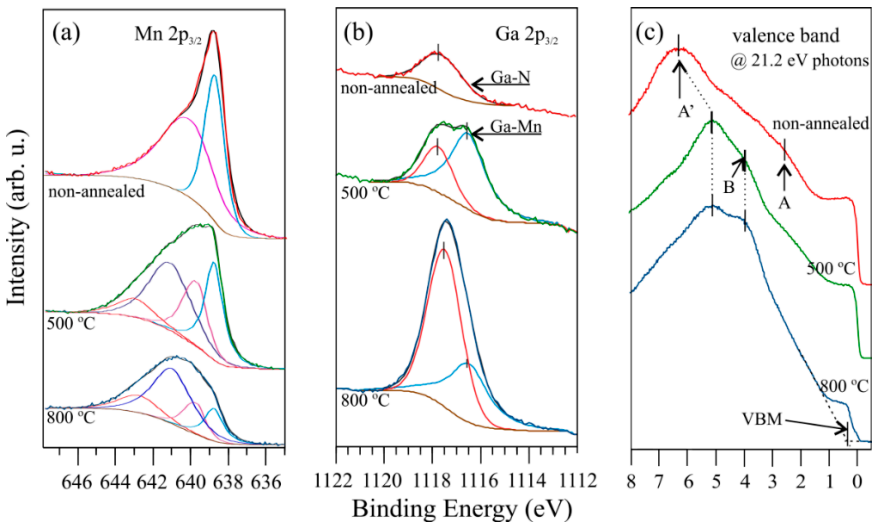


**Figure 11.** Evolution of spectra for (**a**) Mn-2p, (**b**) Ga-2d, and (**c**) valence band for Mn film-covered GaN(0001) with annealing temperature. Data previously published in [23].

Knowing that Mn is dissolved in the substrate, it is interesting how the VB is modified under the influence of annealing. This information was provided by UPS measurements, as shown in Figure 11c. A shape of the VB of Mn film-covered GaN annealed at 500 °C is changed—the feature marked as A disappears, the maximum A′ is shifted towards a low BE and another feature marked with B emerges. Despite the above changes, electron DOS in the vicinity of the $E_F$ is still high, demonstrating a metallic character of the adlayers. Annealing at higher temperature enhances the modification—the feature intensity of A′ decreased and that of B increased. The Fermi edge is still visible, but its intensity is definitely lower. Moreover, it can be seen that the VB of the GaN(0001) Mn doped shifts towards a lower BE and the VBM is 0.4 eV below the $E_F$. This result is very interesting, especially for *p*-GaN crystals, for which the surface Fermi level is far away from the VBM due to band bending at the surface. This leads to a problem with obtaining the Ohmic contacts with this material, as was noted in Ref. [92]. The potential to modify the VB of GaN by dissolving Mn thermal initiation was applied to *p*-GaN(0001) by the author in Ref. [24]. By annealing the Mn film-covered *p*-GaN under UHV conditions, Mn was dissolved in the subsurface layer of the *p*-GaN, similarly as was described above in the case of non-doped GaN. Then, in order to remove the MnGa alloy from the surface, for which UPS showed metallic properties, the system was annealed at 900 °C. After that, the obtained surface was free of the adlayer with the metallic character. However, as a result of high temperature, the obtained surface was faceted. The consequence of such a process is visible in the LEED patterns as extra spots [24] comparable to those presented in Figure 5b.

XPS and UPS results of the work [24] are presented in Figure 12, which shows changes in the Ga-3d and N-1s core level lines caused by the manganese incorporation. The Ga-3d is located at 19.1 and 18.7 eV before and after the Mn incorporation, respectively. Apart from the Ga-3d state, the Mn-3p peak at 47.5 eV is present on the *p*-GaN Mn co-doped, as shown in Figure 12a. The N-1s peak shifts towards a lower BE by 0.4 eV to the position of 396.1 eV after the Mn atoms introduction. So, the shifts of the Ga-3d and N-1s are the same, and a similar observation was also noted in another paper [93], where the Mn implantation by an ion bombardment was applied.

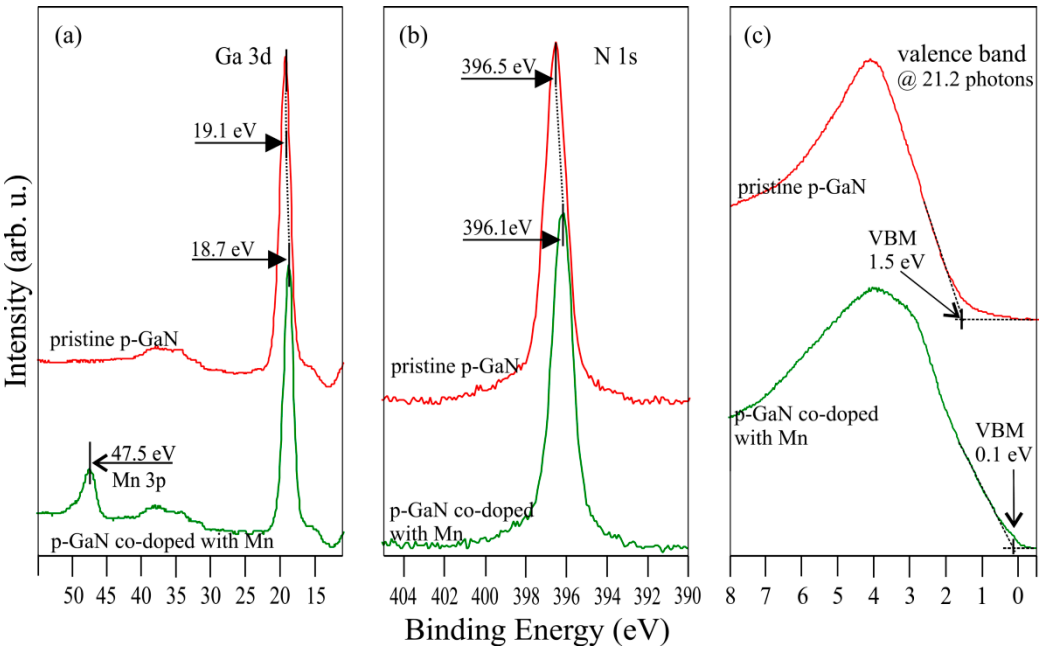


**Figure 12.** XPS spectra of (**a**) Ga-3d with Mn-3p, (**b**) N-1s and (**c**) valence band for pristine *p*-GaN(0001) substrate and co-doped with Mn by thermal annealing of Mn/GaN system. Data previously published in [24].

The presence of Mn atoms in *p*-GaN has a strong impact on the VB and the effects are especially visible nearby the Fermi level. The VBM is 1.5 and 0.1 eV below the $E_F$ for the bare *p*-GaN(0001) surface and the *p*-GaN Mn co-doped, as shown in Figure 12c. The VB of the Mn incorporated *p*-type GaN varies significantly, the electron DOS begins almost at the Fermi level, and its shape is very

similar to that for non-doped (Mn)GaN-like alloy, not included at the edge of the Fermi, as presented in Figure 11c. The widening of the VB in the vicinity of the Fermi level follows from the subsurface layer's modification caused by the incorporation of Mn atoms, leading to the formation of *p*-type (Mn)GaN-like alloy. This is in line with the literature [94–96], where it is shown that the Mn presence in the GaN matrix reconstructs the VB. Another reason that the VBM is practically located by the Fermi level may be surface states deprivation and thus an elimination of band bending on GaN(0001). The band energy diagrams constructed based on the UPS and XPS data for the bare *p*-GaN(0001) and *p*-GaN(0001) co-doped with manganese are shown in Figure 13. There is a clearly noticeable flattening of the band on the surface of the *p*-GaN Mn co-doped with the assumption that the band gap does not change.

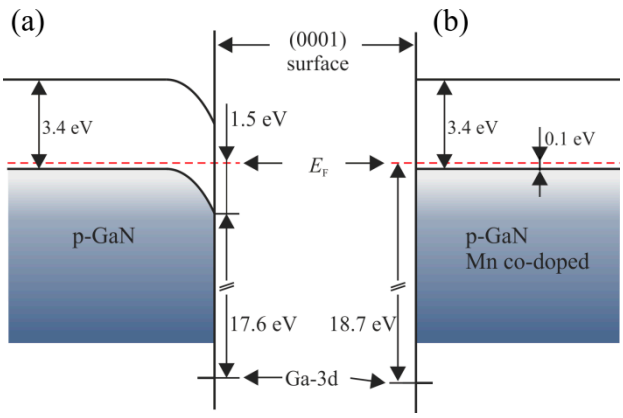


**Figure 13.** Band structure for (**a**) pristine *p*-GaN(0001) surface and (**b**) *p*-GaN(0001) co-doped with Mn assuming that band gap does not change.

### *3.3. Ni on GaN(0001)*

Nickel is a transition metal, in group VIII in the periodic table. The element exhibits good electrical and thermal conductivity properties. Nickel has a density of 8.9 g/cm$^3$, its thermal conductivity is 91 W/(m·°C), and its electrical resistivity amounts to 69 × 10$^{-9}$ Ω·m (at RT). It melts at 1455 °C and its boiling point is 2730 °C (under standard pressure). Ni needs a high temperature to be evaporated in a vacuum and at 930 °C has a vapour pressure of 10$^{-8}$ mbar. Nickel is used for metal contacts with GaN. It can be applied as a single element layer or multilayer with other elements mainly from nickel family, as well as others such as gold, silver etc. [26–28,31]. Structural and topographical analysis of Ni on GaN performed by STM was reported in [97,98]. The first work concerns the growth mode and the interfacial compounds formation. The second focuses on topographic differences between Ni layers deposited at RT, followed by annealing at 650 °C, and Ni layers deposited on the substrate at 650 °C, as a result of which the surface consists mainly of $Ni_3Ga$.The latter procedure gives more strongly dispersed films and is better for catalytic converters, where Ni-Ga alloys can be applied [35,36]. Photoemission experiments were carried out to measure the surface conditions effect on properties of obtained contacts to GaN and the temperature impact on electronic properties of Ni/GaN interfaces [99,100]. In Ref [25], the physicochemical properties of Ni on GaN were investigated with the XPS technique. It was shown that a disordered Ni film grows continuously, in a layer by layer manner (Frank–van der Merwe mode), and the chemical interaction between the adsorbate and the substrate can occur even near RT.

The morphology of Ni film-covered GaN(0001) and morphological changes introduced by annealing as well as SPV impact on XPS and UPS results were presented in the author's papers [29,30]. In these studies, the growth of Ni film by PVD and the characterisation were performed in situ on the *n*- and *p*-type MOCVD GaN(0001) samples. Spectroscopic data were obtained with non-monochromatic excitation lines. The bare surfaces prepared by RTA under UHV conditions had only small amounts of carbon and oxygen contamination and revealed the (1 × 1) structure (confirmed by LEED similar to that in Figure 5a) In these works, the Ni films formed at RT exhibited no diffraction pattern, indicating that they are amorphous. After deposition of Ni film on

the bare *n*-type GaN(0001) surface the Ga-3d core level line shifts towards a lower BE by 0.5 eV to the position 19.9 eV, as shown in Figure 14a. The shift is caused by the Schottky barrier formation. The valence band of the bare and Ni film-covered GaN is presented in Figure 14b. It is clearly seen here that the VBM for the bare GaN(0001) is 2.8 eV, so for the initial surface, it is above the Ga-3d line by $\Delta E$ = Ga-3d − VBM = 17.6 eV. After Ni deposition the Fermi edge is clearly visible, in the spectrum is the characteristic maximum with a BE equals 1.2 eV. The SBH can be simply calculated by the same procedure as applied for Mn films on GaN in the text above (Section 3.2), as well as for Pd films on GaN [101].

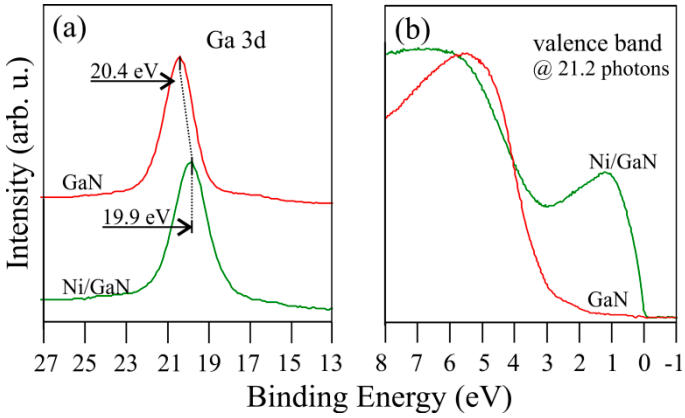


**Figure 14.** Normalized spectra of (**a**) Ga-3d peaks and (**b**) valence band for bare and Ni film-covered GaN(0001) surface. Mean Ni film thickness is 3 nm.

The formula is $\mathrm{SBH}_{\mathrm{GaN}}^{\mathrm{Ni}} = \mathrm{E_g} - \mathrm{VBM}_{\mathrm{GaN}}^{\mathrm{Ni}}$, and the position of $\mathrm{VBM}_{\mathrm{GaN}}^{\mathrm{Ni}}$=$\mathrm{VBM}_{\mathrm{GaN}} - (\mathrm{Ga3d}_{\mathrm{GaN}} - \mathrm{Ga3d}_{\mathrm{GaN}}^{\mathrm{Ni}})$ =2.2 eV, giving the SBH=1.2 eV. The obtained value is consistent with literature, where the SBH is in the range from 0.95 to 1.4 eV. The energy level diagrams of the bare and Ni film-covered GaN(0001) with the SBH constructed based on the UPS and XPS data is shown in Figure 15.

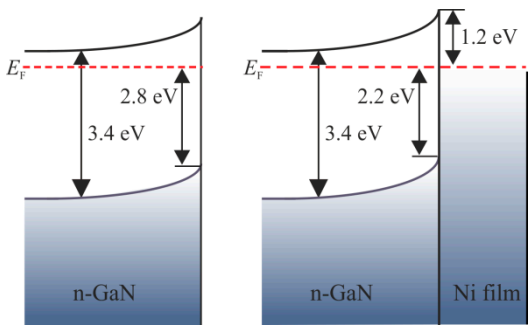


**Figure 15.** Energy band diagrams for Ni film-covered GaN(0001) surface.

The annealing of Ni films on GaN(0001) is interesting from a basic point of view to get a deep insight into the processes occurring on the interface, since this stage is often used in contact creation technology. Temperature treatment of the system by subsequent annealing at 650 °C and then 800 °C leads to a slight shift of the Ni-2p doublet towards a lower BE by 0.15 eV, reaching 870.25 and 853.05 eV for the Ni-$2p_{1/2}$ and Ni-$2p_{2/3}$, respectively. The position of the shake-up satellite changes allowing to monitor Ga-Ni intermixing phases at the surface. The satellite positions are 5.8, 6.2 and 6.7 eV below the parent peak for the non- and annealed surface at 650 °C, followed by 800 °C, respectively, are visible in Figure 16. These relative positions of the satellite are characteristic of the $Ni_3Ga$ and NiGa or $Ni_3Ga_2$ alloys, respectively [102,103]. This does not imply that only these phases of Ga-Ni alloys are presented in the film formed after annealing. It is, with high probability, not a homogeneous film and consists of different phases of alloys and metallic nickel. The results indicate the dominant phases in the film.

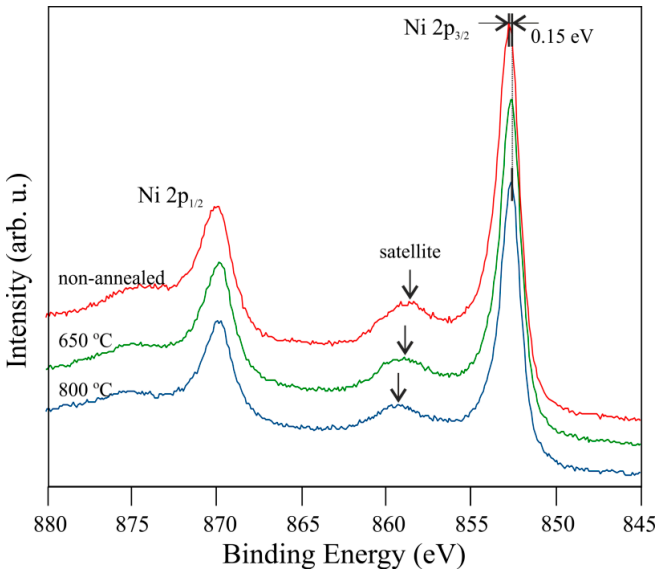


**Figure 16.** XPS spectra of Ni-2p for Ni film-covered GaN(0001) surface showing impact of annealing. Mean Ni film thickness is 3 nm. Data previously published in [29].

Mixing Ni with Ga results from the fact that the latter atoms diffuse from the GaN subsurface layer into the adsorbed Ni film. The result of the intermixing of these two atoms is presented in Figure 17a. The Ga-2p$_{3/2}$ peak splits into two sub-peaks. The sub-peaks at BEs at 1118.3 and 1116.3 eV are attributed to the Ga-N and Ga-Ni bonding. Further annealing at a higher temperature leads to a change in the intensity of the components. The Ga-N bond becomes more visible, indicating that the surface of the substrate is being partially uncovered. Ni atoms are not included into the subsurface layers of GaN, and a substitutional alloy is not formed. The system behaves differently from Mn films on GaN and the mixing appears only on the surface. In addition to temperature-induced changes in core level lines, the alterations also appear in the valence band, as shown in Figure 17b. The spectrum is strongly modified in comparison to the system not annealed. In the vicinity of the $E_F$ are two features at 0.6 and 0.9 eV. The DOSs near the Fermi level for the sample after annealing at both temperatures are very similar. It is worth noting that for the system annealed at 800 °C, the VB of the substrate became visible (marked by an arrow in Figure 17b), which is in line with the changes to the Ga-2p$_{3/2}$ peak. The Fermi edge is similar to that obtained by XPS in [103], which is characteristic of a $Ni_3Ga$ alloy. Therefore, UPS measurements only show one phase of Ni-Ga alloy, regardless of annealing temperature (unlike XPS measurements of the Ni-2p line). Due to the fact that UPS is more surface sensitive than XPS, the results show that the $Ni_3Ga$ alloy is the most dominant phase on the top of the system surface.

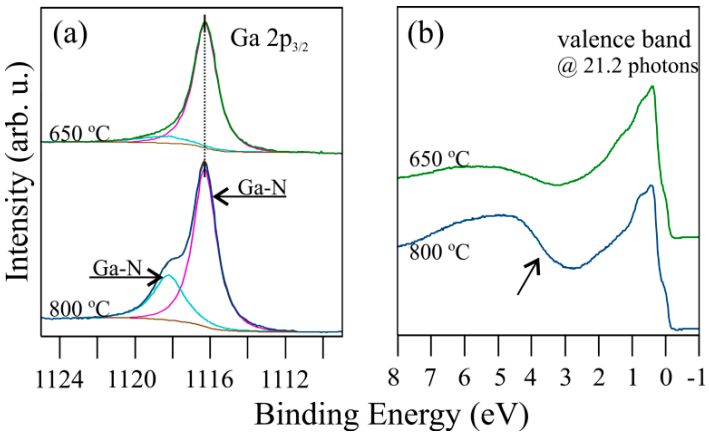


**Figure 17.** (**a**) XPS spectra of Ga-2p, and (**b**) UPS spectra of valence band for Ni film-covered GaN(0001) surface annealed at 650 and 800 °C. Arrow indicates a visible DOS contribution from GaN. Mean film thickness is 3 nm. Data in (a) previously published in [29].

Reconstruction on the surface after annealing is presented in Figure 18. LEED patterns from Ni film annealed at 650 °C show strong sharp spots corresponding to the Ni(111)-(√3 × √3)*R*30° structure with a lattice constant of 2.58 Å and after annealing at 800 °C reveal sharp diffraction spots of the Ni(111)-(2 × 2) and GaN(0001)-(1 × 1) structures. The presence of spots corresponding to GaN (0001)-(1 × 1) shows that further Ni-Ga alloying is accompanied by coalescence and, consequently, partial opening of the film and uncovering the substrate surface, which is consistent with the spectroscopic observations.

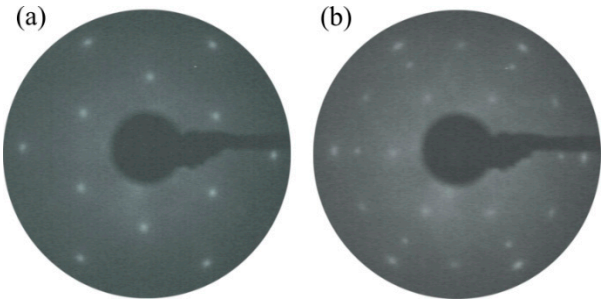


**Figure 18.** LEED patterns (90 eV) for the Ni film-covered GaN(0001) after annealing at (**a**) 650 and (**b**) 800 °C. The three domains of the square structure of MnGa alloy and the (1 × 1) of the hexagonal structure of GaN(0001) substrate are marked. Mean film thickness is 3 nm. Data previously published in [29].

When semiconductors are exposed to photons with a higher energy than their forbidden gaps, electron–hole pairs are formed. The generation of an electron hole can also take place in metal/semiconductor systems, especially in the case of thin coating systems [104], and as a consequence, may result in an appearance of a quasi-Fermi level. Such effect in the case of the Ni film on p-type GaN(0001) was described in Ref. [30] and is presented below in the text. Evolutions of the Ga-3d and Ni-2p$_{3/2}$ core level lines after Ni deposition on p-type GaN(0001) surface followed by annealing are shown in Figure 19. The Ga-3d peak is located at a BE of 18.9 eV for the bare p-GaN(0001) surface and shifts towards a higher BE to the position 19.6 eV after the Ni film deposition. According to the Mn/GaN (Section 3.2), as well as Ni/*n*-GaN systems described above in the text, it is obvious that the shift is related to the Schottky barrier formation. The SBH of Ni on p-GaN for electrons is $\mathrm{SBH}_{\mathrm{pGaN}}^{\mathrm{Ni}} = \mathrm{E_g} - \mathrm{VBM}_{\mathrm{GaN}}^{\mathrm{Ni}}$, and the position of $\mathrm{VBM}_{\mathrm{GaN}}^{\mathrm{Ni}}$=1.9 eV (based on the Ga-3d shift), giving the SBH=1.5 eV. The value of 1.9 eV is the magnitude of SBH for holes. However, after annealing of the system at 800 °C, the Ga-3d peak moves to its initial position, as shown in Figure 19a, which is unusual. Meanwhile, the Ni-2p$_{3/2}$ core level line has a BE of 852.6 eV for the as-deposed film and shifts by 1.0 eV towards a lower BE following annealing, as shown in Figure 19b.

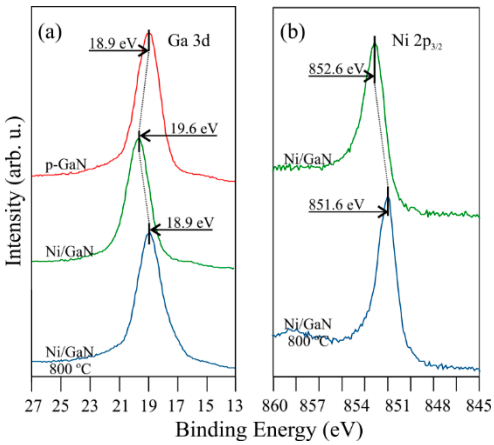


**Figure 19.** XPS spectra of (**a**) Ga 3d and (**b**) Ni 2p$_{3/2}$ for the bare and Ni film-covered *p*-GaN(0001) before and after annealing. Mean film thickness is 1 nm. Data previously published in [30].

It would seem that such a large shift of the Ni line after annealing occurred as a result of a chemical reaction; however, as UPS measurements show, this interpretation is completely wrong. Spectra of the valence band for the bare and Ni film-covered *p*-GaN(0001) before and after annealing at 800 °C are shown in Figure 20. The VBM of the *p*-GaN sample is 1.2 eV below the $E_F$, which gives $\Delta E$ = Ga-3d – VBM = 17.7 eV. After the deposition of the thin Ni film of mean thickness of 1 nm a DOS nearby the $E_F$ increases - the Fermi edge of the Ni film is clearly visible. The VB of the *p*-GaN is also noticeable in the spectrum, although shifted—its VBM now lies at 1.9 eV. This shift, similar as for the Ga-3d, is related to the electron charge transfer at the interface causing the Schottky barrier with a SBH for hole carriers amounts to the above value of 1.9 eV. After annealing, the VBM returns to the starting position, similarly to the Ga-3G peak behaviour. The DOS of the Ni film is still visible but above the Fermi level of energy analyzer—a quasi-Fermi level appeared at a BE of −1.0 eV. The separation of the Fermi level in the substrate and the thin Ni film causes the shifts of the Ga-3d and Ni-2p$_{3/2}$ core level line. The situation is well illustrated in Figure 21.

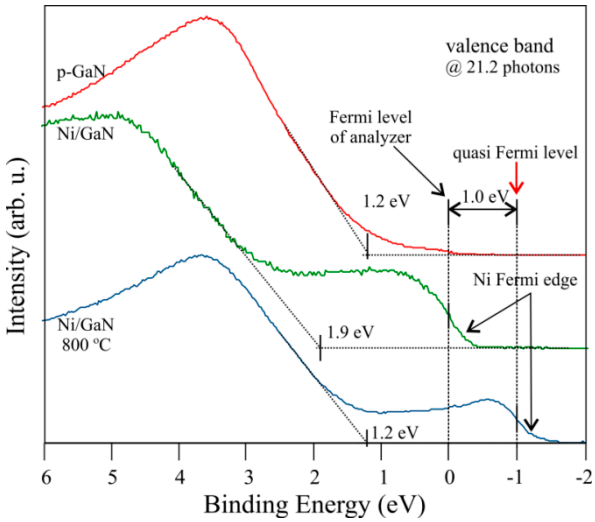


**Figure 20.** UPS spectra of the valence band for ~~(a)~~ bare, and Ni thin film-covered *p*-GaN(0001) surface ~~(b)~~ before and ~~(c)~~ after annealing. Mean film thickness is 1 nm. Data ~~in~~ previously published in [30].

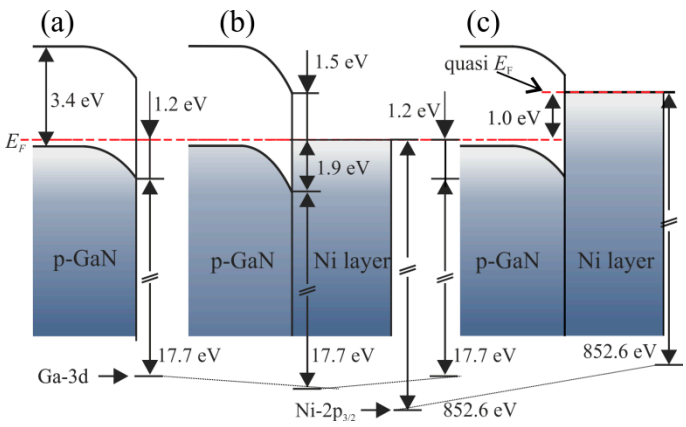


**Figure 21.** Band diagrams for (**a**) bare, and Ni thin film-covered *p*-GaN(0001) surface (**b**) before and (**c**) after annealing.

The presence of the quasi Fermi level follows from that the uncovering of the GaN surface after annealing exposes the phase boundary for illumination by photons whose energy is much higher than the forbidden gap of the GaN, resulting in electron-hole pairs being generated there. The *p*-GaN(0001) surface is more negatively charged, compared to the system not annealed (Figure 21b), due to a holes transport from the nearby site of the interface to the grounded part of the sample. The Ni film-covered substrate after annealing is in the same condition as the bare surface (Figure

21a,c). Electrons from the valence band near to the phase boundary are ejected into the conduction band of the substrate which is bent downwards, so there is no barrier for them from the metal film side, and they may flow down to the Ni film. Thus, this part of the system is more negatively charged. The above text regarding Ni on *p*-GaN is a good example, showing that some shifts in core level lines observed after annealing do not necessarily have to be the result of an interfacial chemical reaction and may be a consequence of other effects.

### *3.4. As and Sb on GaN(0001)*

Arsenic and antimony are semi-metals belonging to nitrite family, in group V in the periodic table. Both of these chemical elements exhibit poor electrical and thermal conductivity properties. Arsenic in crystal structure has poor metallic properties; however, in an amorphous form, it exhibits semiconductor properties and has a forbidden gap of 1.2 eV [67]. As has a density of 5.75 g/cm$^3$, its thermal conductivity is 50 W/(m·K), and its electrical resistivity amounts to 3 × 10$^{-7}$ Ω·m (at RT). It does not melt and starts to sublimate at 615 °C (under standard pressure). It easily evaporates in a vacuum starting at 107 °C with a vapour pressure of 10$^{-8}$ mbar but in a form of various clusters. To eliminate this effect, a special evaporation source with a cracker is needed. Antimony has a density of 6.69 g/cm$^3$, its thermal conductivity is 24 W/(m·K), and its electrical resistivity amounts to 4 × 10$^{-7}$ Ω·m (at RT). It melts at 630 °C and its boiling point is 1635 °C (both values refer to standard pressure). Like arsenic, antimony easily evaporates in a vacuum starting at 279 °C with a vapour pressure of 10$^{-8}$ mbar and also in a form of various clusters. Both of these elements are used in the electronic industry as a part of semiconductor compound (e.g., GaAs, InSb) or as *n*-type dopants for the semiconductor IV-group. Furthermore, they were attempted to be used as surfactants to improve the quality of GaN layers grown by MBE [42–47], as well as to form new electronic materials such as GaN(As) and GaN(Sb) alloys. The introduction of As or Sb into GaN causes a modification of the electronic structure of the host material. Both elements cause narrowing of the forbidden gap, in addition, arsenic shifts the VB upwards [48–54].

Surface study on the interaction of As with the GaN(0001) using XPS with monochromatic Al line and reflection of high-energy electron diffraction (RHEED) were described in the author's work [57]. The reason for this research is the potential use of arsenic as a means to modify the electronic properties of surfaces. The growth of As film by PVD with a cracker source and characterisation were performed in situ on non-doped MOCVD GaN(0001). The initial bare surface prepared by RTA reveals a very small amount of carbon (at the limit of XPS detection) and no oxide contaminant. RHEED exhibits sharp and bright diffraction patterns corresponding to the (1 × 1) structure (not shown). During the growth, the signal of the RHEED patterns decreases with an overlayer thickness of As films. For coatings equal to 2 nm and higher, the patterns disappear completely, suggesting that the film is amorphous. The Ga-3d, As-2p$_{3/2}$ core level lines and the valence band prior to and after the deposition of the ~5 nm thick As film are presented in Figure 22.

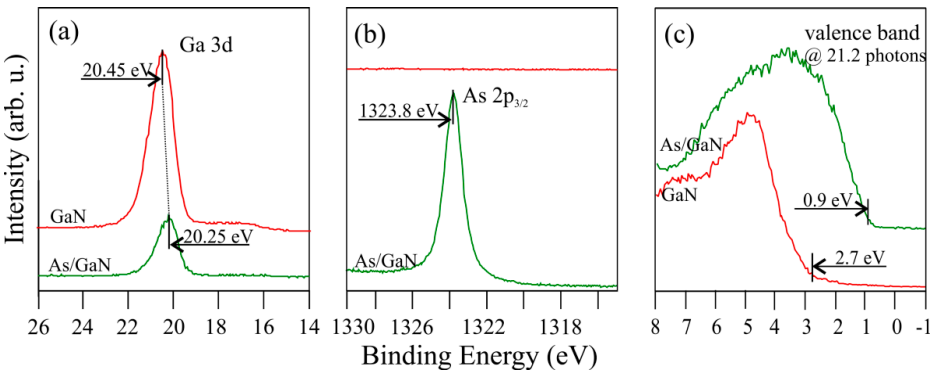


**Figure 22.** XPS spectra of (**a**) Ga-3d, (**b**) As-2p$_{3/2}$ and (**c**) UPS spectra of valence band for the bare and As film-covered GaN(0001). Mean film thickness is ~5 nm. Data previously published in [57].

After arsenic deposition on the bare GaN(0001) surface, the Ga-3d core level line shifts towards a lower BE by 0.2 eV to a position of 20.25 eV. The As-p$2_{3/2}$ emerges at a BE of 1323.3 eV and corresponds to As-As bonds [105]. The valence band of the bare GaN(0001) surface is characteristic of typical non-doped GaN. The VBM lies 2.7 eV below the $E_F$ and the energetic distance from it to the Ga-3d state is $\Delta E$ = Ga-3d − VBM = 17.7 eV. The DOS of the As film does not start at the Fermi level, as shown in Figure 22c. The edge is shifted towards a higher BE meaning that the amorphous layers have semiconductor character for which the VBM is 0.9 eV below the $E_F$. The shift of the Ga-3d peak, shown in Figure 22a, is caused by electrons transfer at the interface, similar to the metal/GaN systems described above in the text (Section 3.1 and 3.2). However, in this case, instead of SBH, the valence band offset ($\Delta E_V$) at the phase boundary can be estimated. It can be done basing on a method described in Ref. [106]. The formula is $\Delta E_V = E_{V\text{-}As2p}(As) - E_{V\text{-}Ga3d}(GaN) - \Delta E_{As2p,Ga3d}$, where $E_{V\text{-}As3d}(As)$ and $E_{V\text{-}Ga3d}(GaN)$ are the Ga-3d, the As-$2p_{3/2d}$ positions relative to the VBM of GaN and As film. Those values are 17.7 and 1322.9 eV and $\Delta E_{As3d,Ga3d}$ is the energy difference between the As-$2p_{3/2}$ and Ga-3d levels when both peaks are visible after the As/GaN interface creation, it amounts to 1303.55 eV. The $\Delta E_V$ for the As/GaN interface is 1.65 eV. This means that the valence band of As is above the VB of GaN by that value. The conduction band offset ($\Delta E_C$) can be also evaluated with the formula $\Delta E_C = E_g(As) + \Delta E_V - E_g(GaN)$, where values of 1.2 and 3.4 eV are used for the forbidden gap of the As film [67] and GaN, respectively. The $\Delta E_c = -0.55$ eV. The '-' sign indicates that the conduction band of As is below that of the GaN. These values allow to us construct an energy sketch for the As/GaN phase boundary, as shown in Figure 23.

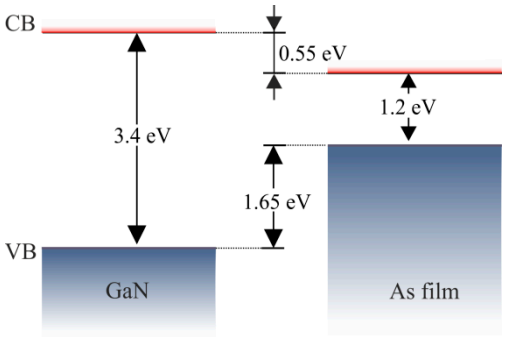


**Figure 23.** Bands diagram demonstrating valence and conduction band offsets for As film-covered GaN(0001) surface.

The relatively low As sublimation temperature under UHV conditions should allow As to easily escape from the surface of GaN (0001). Examination of the effect of temperature on the As/GaN system shows that annealing at temperatures below and equal to 200 °C does not introduce significant changes. The As-2p peak intensity decreases slightly after annealing at 200 °C. This is surprising, because at 200 °C arsenic has a relatively high vapour pressure of $10^{-4}$ mbar. After annealing at 300 °C, As does not desorb completely from the surface. The As-$2p_{3/2}$ core level line shifts slightly from 1323.8 to 1323.65 eV and for temperatures in the range from 350 to 500 °C the peak shifts further, reaching the positions of 1323.3 eV, as shown in Figure 24. This indicates that there has been a chemical interaction of arsenic with the GaN(0001) surface. However, the As-$2p_{3/2}$ core level line lies at a higher BE than the As-Ga bonding. Therefore, it is possible that arsenic may interact with the surface in the form of $As_2$, as considered in Ref. [44]. Repeating series (As deposition + annealing) does not create new surface alloys on GaN (0001), as in the case of the previously described Ni/GaN system (Section 3.2) or the Pd/GaN system [34]. The condition of the interface remains unchanged, i.e., the XPS lines from the substrate and the adsorbate do not change. In addition the amount of the fraction $As_2$-GaN(0001) remains unchanged. This is due to the vapour pressure of the adsorbate being much higher than that of gallium (metallic gallium has a vapour pressure of $10^{-4}$ mbar at 900 °C). So, arsenic atoms escape into the vacuum and have no chance to react with the segregated gallium on the surface. An example of changes introduced in the valence band by annealing at 400 °C is shown in Figure 24b. The As film thickness for this stage is 0.25 nm.

Taking the As density, 1 Å = 4.62 × $10^{14}$ As·$cm^{-2}$ and one monolayer (ML) on GaN(0001) surface corresponds to a density of 1.14 × $10^{15}$ atoms·$cm^{-2}$. This gives a coverage of As equal to 1 ML. This coverage also explains the lack of growth of the residual arsenic after the subsequent cycles (deposition + annealing), since there is no site where it could chemically interact with the GaN(0001) surface.

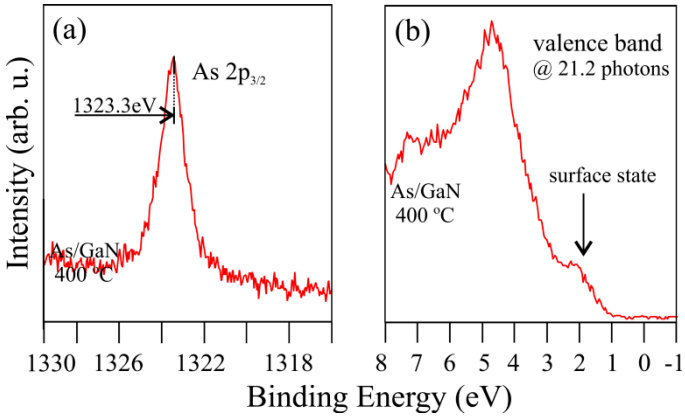


**Figure 24.** XPS spectra of (**a**) As-2$p_{3/2}$ and (**b**) UPS spectra of valence band for the annealed As film-covered GaN(0001) at 400 °C. Amount of residual arsenic is 1 ML. Data previously published in [57].

The surface DOS (SDOS) emerges at a position of 2.2 eV below the Fermi level. Its highest occupied state is found to be at 1.05 eV. Furthermore, the VBM for the system shifts upwards by 0.2 eV, compared to the bare surface, and lies 2.5 below the $E_F$. For this stage of the experiment, RHEED patterns exhibit the clear (1 × 1) structure and the Ga-3d is shifted to 20.3 eV. The energy diagrams constructed for the initial bare and As-modified GaN(0001) surfaces are presented in Figure 25.

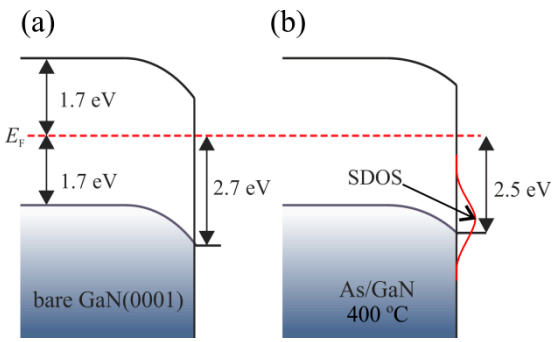


**Figure 25.** Energy diagrams for (**a**) bare GaN(0001) and (**b**) annealed As film-covered GaN(0001) surface at 400 °C.

The SDOS is very visible, even for the system annealed at 500 °C. Further annealing in a temperature range of 600–700 °C of the already annealed system reduces the amount of arsenic. However, this does not completely remove arsenic from the surface. At 700 °C, the As-2$p_{3/2}$ line shifts to a BE of 1322.85 eV, which corresponds to As-Ga bonds in GaAs crystals [105,107], revealing that arsenic atoms are no longer present at the surface as $As_2$. The residues of the SDOS can still be slightly distinguished in the valence band spectrum. Therefore, proves that the SDOS is associated with As present on the GaN surface.

The interaction of Sb adsorber with the GaN(0001) surface and morphological changes caused by post-deposition annealing were studied in Ref. [58]. The growth of As film by PVD and the surface investigation were carried out in situ on the Mg-doped, *p*-type, MOCVD GaN(0001) surface. The initial surface was prepared by annealing under UHV conditions. After that, the clean surface reveals a very small amount of oxygen and no carbon (C KLL). LEED exhibits sharp and bright diffraction patterns corresponding to the (1 × 1) structure (similar to that in Figure 5a). LEED does not show diffraction patterns for Sb films deposited at RT on the *p*-type GaN(0001) surface. This

indicates that Sb layers are amorphous. For the bare surface, the Ga-3d peak is located at 19.5 eV and after deposition of the Sb film, 5 nm thick, the line shifts towards a higher BE to the position 20.5 eV, as shown in Figure 26a. The Sb-4d core level line is located at a BE of 32 eV. The shift of Ga-3d results from the Schottky barrier formation. The VBs of the bare and Sb film-covered GaN(0001) surface are presented in Figure 26b. The VBM is located 1.5 eV below the $E_F$ for the bare GaN(0001), so it is above the Ga-3d peak by $\Delta E$ = Ga-3d – VBM = 17.6 eV. After Sb deposition, the Fermi edge is clearly visible with a characteristic maximum at 1.6 eV, and the spectrum is similar to that observed for Sb/SiC system in Ref. [108].

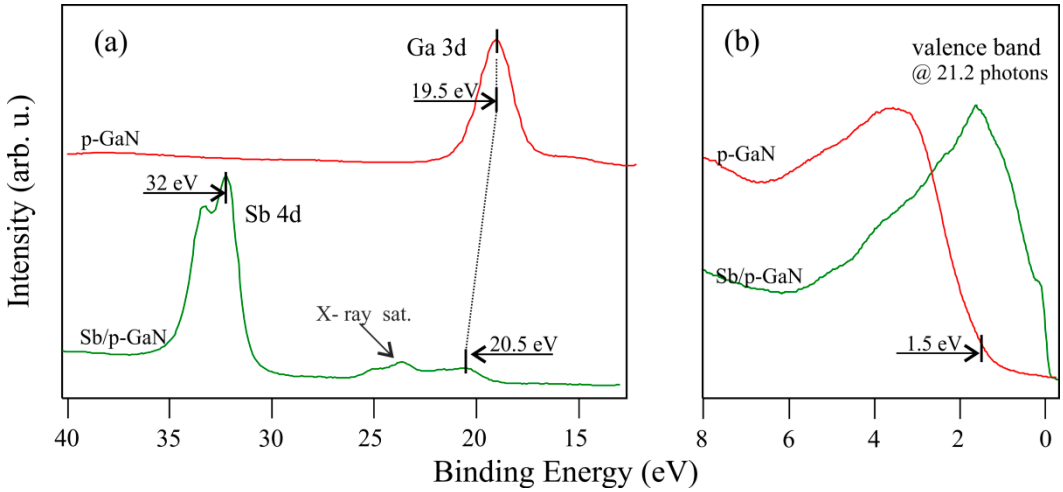


**Figure 26.** XPS spectra of (**a**) Ga-3d, Sb-3d and (**b**) UPS spectra of valence band for the bare and Sb film-covered GaN(0001). Mean thickness of film is 5 nm. Data previously published in [57].

The SBH can be calculated by the same procedure as in the case of Mn or Ni films on GaN in the text above (Sections 2.2 and 2.3). The SBH for electron is $\mathrm{SBH}_{\mathrm{GaN}}^{\mathrm{Sb}} = \mathrm{E_g} - \mathrm{VBM}_{\mathrm{GaN}}^{\mathrm{Sb}}$, and the position of $\mathrm{VBM}_{\mathrm{GaN}}^{\mathrm{Sb}}$=$\mathrm{VBM_{GaN}} - (\mathrm{Ga3d_{GaN}} - \mathrm{Ga3d}_{\mathrm{GaN}}^{\mathrm{Sb}})$ =2.5 eV, giving the SBH=0.9 eV, while the value of 2.5 eV it is the SBH for holes. The bands diagrams for the bare and Sb film-covered GaN(0001) are illustrated in Figure 27.

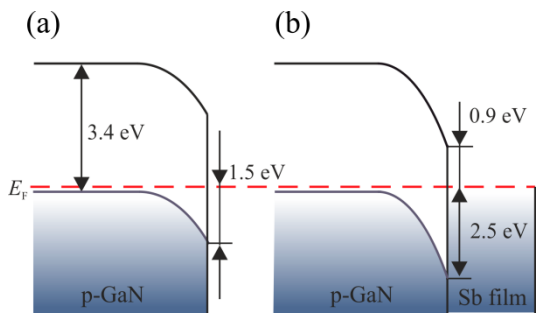


**Figure 27.** Bands diagram for (**a**) bare and (**b**) Sb film-covered GaN(0001) surface.

Sb atoms easily desorb from surfaces under UHV conditions, starting at about 280 °C [108]. Therefore, annealing of the Sb/GaN system at 400 °C should lead to complete desorption of Sb atoms from the GaN(0001) surface. However, the investigation shows a presence of the Sb-3d peak in the XPS spectrum. The position of the Sb-4d remains unchanged relative to the metallic Sb, which may suggest no chemical interaction with the surface; however, the BE of 32 eV is characteristic of the Ga-Sb binding [109]. Considering the annealing temperature and the position of the Sb-4d, this all indicates that the residual As on the surface is rather in a chemical compound of Ga. So, the system under the influence of annealing behaves similarly to the As/GaN. The Ga-3d state shifts from 20.5 eV towards a lower BE to 19.9 eV, as shown in Figure 28a. The thickness of the residual Sb film is 0.25 nm. Taking the Sb density, 1 Å = 3.31 × $10^{14}$ Sb·cm$^{-2}$, this gives a coverage of Sb equal to

~0.7 ML. The UPS spectrum shows a restoration of the valence band of a semiconductor type, with no sign of DOS, unlike in the case of the As/GaN system. The VBM lies at 1.6 eV below the $E_F$, as shown in Figure 28b. In addition to changes in the VBM, the small amount of As strongly modifies the vacuum level, which is smaller by 1.2 eV compared to the bare surface [57].

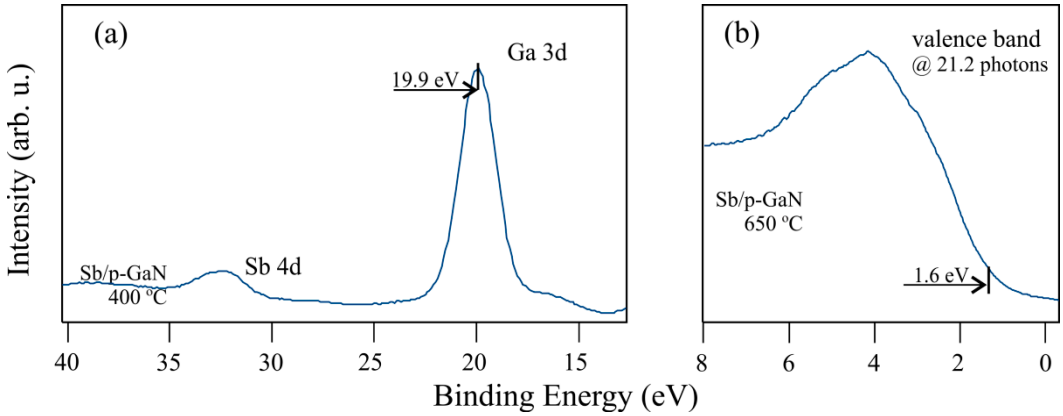


**Figure 28.** XPS spectra of (**a**) Ga-3d, Sb-3d and (**b**) UPS spectra of valence band for annealed Sb film-covered GaN(0001) surface at 400 °C. Amount of residual arsenic is ~0.7 ML. Data previously published in [57].

## 4. Summary

Photoelectron spectroscopies (XPS, UPS) were used to investigate properties of bare and film-covered GaN(0001) surfaces.

The bare GaN(0001) was characterized with different X-ray excitation sources, i.e., non-monochromatic Mg $K_\alpha$ (1253.6 eV), non- and monochromatic Al $K_\alpha$ (1486.7 eV). Their influence on the shapes of the core level lines and valence band are found. The type of X-ray source has a particularly large impact on the shape of the N-1s line due to the overlap of the Auger lines that occur for photons with an energy of 1487.7 eV. Significant changes are also observed in the valence band, caused by overlapping with X-ray satellites in the case of non-monochromatic sources. Binding energy positions of Auger lines vs. X-ray sources are shown. Electronic properties of non- and various doped GaN(0001) surfaces studied by UPS are presented. The valence band maxima lie 2.7 eV below the Fermi level for non-doped GaN and, in the case of doped materials, they are at 3.1 and 1.5 eV for the n- and *p*-type semiconductor, respectively.

Physical and chemical properties of thin films on GaN(0001), including several elements—manganese, nickel, arsenic and antimony—were described. Photoelectron spectroscopies were also employed to determine the Schottky barrier height at the formed interfaces. The systems were created in situ on the substrates cleaned by annealing under UHV conditions and adsorbates were evaporated from a Knudsen-like cells. No evidence of epitaxial growth of the films at RT was found.

The investigation of manganese films on GaN(0001) shows that the Schottky barrier height of the interface amounts to 1.20 eV. A chemical interaction of Mn atoms with the substrate at RT is excluded. Annealing the system results in morphological changes. Mn atoms and Ga intermix at the interface. Two effects are found: (i) segregated Ga atoms diffuse into Mn, forming MnGa surface alloy; (ii) Mn atoms move in the opposite direction, toward the inside of the substrate, and consequently form (Mn, Ga)N-like alloy. MnGa surface alloy stays on the GaN(0001) after annealing up to 800 °C, achieving a domain structure epitaxially oriented relatively to the GaN(0001) substrate. Annealing at a higher temperature can result in removing the MnGa adlayer, but the effect of replacing gallium with manganese atoms in the sublayers of GaN is still visible. It leads to a strong modification of the valence band. The valence band maximum of *p*-GaN after thermal desorption of the MnGa surface alloy is strongly shifted upwards from 1.5 to 0.1 eV. This result is promising as a stage of preparation of the substrate for Ohmic contacts with *p*-GaN.

The studies on nickel films on GaN(0001) surfaces show that the Schottky barrier height of the interface with *n*-type semiconductor amounts to 1.20 eV and with *p*-type is 1.5 and 1.9 eV for electrons and holes, respectively. Annealing the Ni/GaN interface causes uncovering of the substrate surface. A coalescence of grainy Ni films occurs. Moreover, Ni-Ga surface alloying is exhibited. Ga diffuses into a Ni film and intermixes with it. $Ni_3Ga$ is found to be the dominant alloying phase. Further annealing at a higher temperature leads to the formation of a more Ga-rich alloy phase. It is recognized as NiGa or $Ni_3Ga_2$.

The Ni/p–GaN interface investigation revealed that the XPS and UPS measurements themselves may affect the electronic structure of the system. Surface conditions of the system were found in which electrons ejected by X-rays or UV penetrate into the metal part of the interface, leading to the film being charged, the consequence of which is the appearance of quasi-Fermi level and shifting the film's core level lines. This result is a good example of the fact that some shifts of XPS peaks observed after annealing metal/semiconductor systems may be a consequence of other effects than chemical interactions. Therefore, to explain the reason for this shift, core level measurements are insufficient and electrons from a valence band should also be monitored.

The study of arsenic films on GaN(0001) shows that the amorphous films exhibit a semiconductor character. The valence band offset is determined to be 1.65 eV and the conduction band offset is -0.55 eV relative to the conduction band of the substrate. A chemical interaction of As atoms with the substrate at RT is excluded. Annealing the system results in an arsenic desorption, although not completely. The residual As atoms chemically interact with the GaN(0001) surface, probably in the form of $As_2$-Ga. Further annealing at a higher temperature means that the As remainders are supposed to chemically react with the surface in the form of As-Ga. The presence of As atoms at the GaN(0001) surface causes a modification of the valence band – SDOS appears.

The investigation of antimony films on *p*-GaN(0001) shows that the Schottky barrier height of the interface is 0.9 and 2.50 eV for electrons and holes, respectively. The annealing of the system causes an antimony desorption; however, as in the As/GaN system, Sb atoms are not completely removed. Despite the lack of shift of the Sb-4d, it is assumed that residual Sb atoms might be reacted with the substrate since the temperature is too high for metallic Sb atoms to survive on the surface.

**Acknowledgments:** The work was supported by the University of Wrocław. Some results shown in this paper were obtained as part of the project FNP—Team Tech/2016-3/16 carried out at PORT. The author would like to thank all the scientists with whom he had the opportunity to cooperate on the topics presented in this work. The author would also like to thank A. Sabik and K. Świstak for correcting the manuscript.

## References

1. Doverspike, K.; Pankove, J. Chapter 9 Doping in the III-Nitrides. In *Future Directions in Silicon Photonics*; Elsevier BV: Amsterdam, The Netherlands, 1997; Volume 50, pp. 259–277.
2. Nakamura, S.; Senoh, M.; Mukai, T. Highly P-Typed Mg-Doped GaN Films Grown with GaN Buffer Layers. *Jpn. J. Appl. Phys.* **1991**, *30*, L1708–L1711, doi:10.1143/jjap.30.l1708.
3. Nakamura, S.; Mukai, T.; Senoh, M.; Iwasa, N. Thermal Annealing Effects on P-Type Mg-Doped GaN Films. *Jpn. J. Appl. Phys.* **1992**, *31*, L139–L142, doi:10.1143/jjap.31.l139.
4. Khan, M.A.; Chen, Q.; Shur, M.S.; Dermott, B.; Higgins, J.; Burm, J.; Schaff, W.; Eastman, L. GaN based heterostructure for high power devices. *Solid-State Electron.* **1997**, *41*, 1555–1559, doi:10.1016/s0038-1101(97)00104-4.
5. Yao, T.; Hong, S.-K. (Eds.). *Oxide and Nitride Semiconductors: Processing, Properties, and Applications*; Springer: Berlin/Heidelberg, Germany, 2009. Available online: www.springer.com/us/book/9783540888468 (accessed on 24 January 2019).
6. Flack, T.J.; Pushpakaran, B.; Bayne, S.B. GaN Technology for Power Electronic Applications: A Review. *J. Electron. Mater.* **2016**, *45*, 2673–2682, doi:10.1007/s11664-016-4435-3.
7. Qian, H.; Lee, K.; Vajargah, S.H.; Novikov, S.; Guiney, I.; Zaidi, Z.; Jiang, S.; Wallis, D.; Foxon, C.; Humphreys, C.; et al. Novel GaN-based vertical heterostructure field effect transistor structures using crystallographic KOH etching and overgrowth. *J. Cryst. Growth* **2017**, *459*, 185–188, doi:10.1016/j.jcrysgro.2016.12.025.

8. Medjdoub, F.; Iniewski, K. *Gallium Nitride (GaN)*; Informa UK Limited: London, UK, 2017.
9. Mochizuki, K. *Vertical GaN and SiC Power Devices*; Artech House: Norwood, MA, USA, 2018.
10. Coffie, R.L. High Power High Frequency Transistors: A Material's Perspective. In *High-Frequency GaN Electronic Devices*; Springer Science and Business Media LLC: Berlin/Heidelberg, Germany, 2019; pp. 5–41.
11. Janicki, L.; Kunert, G.; Sawicki, M.; Piskorska-Hommel, E.; Gas, K.; Jakiela, R.; Hommel, D.; Kudrawiec, R. Fermi level and bands offsets determination in insulating (Ga,Mn)N/GaN structures. *Sci. Rep.* **2017**, *7*, 41877, doi:10.1038/srep41877.
12. Gas, K.; Domagala, J.Z.; Jakieła, R.; Kunert, G.; Dluzewski, P.; Piskorska-Hommel, E.; Paszkowicz, W.; Sztenkiel, D.; Winiarski, M.J.; Kowalska, D.; et al. Impact of substrate temperature on magnetic properties of plasma-assisted molecular beam epitaxy grown (Ga,Mn)N. *J. Alloy. Compd.* **2018**, *747*, 946–959, doi:10.1016/j.jallcom.2018.03.056.
13. Pearton, S.J.; Abernathy, C.; Norton, D.; Hebard, A.F.; Park, Y.; Boatner, L.A.; Budai, J.D. Advances in wide bandgap materials for semiconductor spintronics. *Mater. Sci. Eng. R Rep.* **2003**, *40*, 137–168, doi:10.1016/s0927-796x(02)00136-5.
14. Dietl, T.; Ohno, H. Dilute ferromagnetic semiconductors: Physics and spintronic structures. *Rev. Mod. Phys.* **2014**, *86*, 187–251, doi:10.1103/revmodphys.86.187.
15. Qi, Y.; Sun, G.F.; Weinert, M.; Li, L. Electronic structures of Mn-induced phases on GaN(0001). *Phys. Rev. B* **2009**, *80*, 235323, doi:10.1103/physrevb.80.235323.
16. Wang, K.; Takeuchi, N.; Chinchore, A.V.; Lin, W.; Liu, Y.; Smith, A.R. Two-dimensional Mn structure on the GaN growth surface and evidence for room-temperature spin ordering. *Phys. Rev. B* **2011**, *83*, 165407, doi:10.1103/physrevb.83.165407.
17. Cui, Y.; Li, L. A (10 × 10) domain wall structure induced by Mn adsorption on the pseudo-(1 × 1) surface of GaN(). *Surf. Sci.* **2003**, *522*, L21–L26, doi:10.1016/s0039-6028(02)02400-7.
18. Dumont, J.; Kowalski, B.; Pietrzyk, M.; Seldrum, T.; Houssiau, L.; Douhard, B.; Grzegory, I.; Porowski, S.; Sporken, R. Atomically flat GaMnN by diffusion of Mn into GaN(). *Superlattices Microstruct.* **2006**, *40*, 607–611, doi:10.1016/j.spmi.2006.07.028.
19. Chinchore, A.; Wang, K.; Shi, M.; Liu, Y.; Smith, A.R. Spontaneous formation of quantum height manganese gallium islands and atomic chains on N-polar gallium nitride(0001). *Appl. Phys. Lett.* **2012**, *100*, 61602, doi:10.1063/1.3682487.
20. Kowalik, I.A.; Kowalski, B.; Orlowski, B.; Lusakowska, E.; Iwanowski, R.; Mickevičius, S.; Johnson, R.; Grzegory, I.; Porowski, S. Photoemission study of Mn/GaN. *Surf. Sci.* **2004**, *566*, 457–461, doi:10.1016/j.susc.2004.05.085.
21. Hwang, J.I.; Osafune, Y.; Kobayashi, M.; Ebata, K.; Ooki, Y.; Ishida, Y.; Fujimori, A.; Takeda, Y.; Okane, T.; Saitoh, Y.; et al. Depth profile high-energy spectroscopic study of Mn-doped GaN prepared by thermal diffusion. *J. Appl. Phys.* **2007**, *101*, 103709, doi:10.1063/1.2732679.
22. Grodzicki, M.; Mazur, P.; Krupski, A.; Ciszewski, A. Studies of early stages of Mn/GaN(0001) interface formation using surface-sensitive techniques. *VAC* **2018**, *153*, 12–16, doi:10.1016/j.vacuum.2018.03.059.
23. Grodzicki, M.; Mazur, P.; Brona, J.; Ciszewski, A. MnGa and (Mn,Ga)N-like alloy formation during annealing of Mn/GaN(0001) interface. *Appl. Surf. Sci.* **2019**, *481*, 790–794, doi:10.1016/j.apsusc.2019.03.121.
24. Grodzicki, M.; Mazur, P.; Sabik, A. Electronic properties of p-GaN co-doped with Mn by thermal process: Surface studies. *Surf. Sci.* **2019**, *689*, 121460, doi:10.1016/j.susc.2019.121460.
25. Bermudez, V.M.; Kaplan, R.; Khan, M.A.; Kuznia, J.N. Growth of thin Ni films on GaN(0001)-(1 × 1). *Phys. Rev. B* **1993**, *48*, 2436–2444, doi:10.1103/physrevb.48.2436.
26. Schmitz, A.C.; Ping, A.T.; Khan, M.A.; Chen, Q.; Yang, J.W.; Adesida, I. Schottky barrier properties of various metals on n-type GaN. *Semicond. Sci. Technol.* **1996**, *11*, 1464–1467, doi:10.1088/0268-1242/11/10/002.
27. Schmitz, A.; Ping, A.; Adesida, I.; Khan, M.A. Schottky Barrier Heights of Ni, Pt, Pd, and Au on n-type GaN. *MRS Proc.* **1995**, *395*, 831–835.
28. Rickert, K.A.; Ellis, A.; Kim, J.K.; Lee, J.-L.; Himpsel, F.J.; Dwikusuma, F.; Kuech, T.F. X-ray photoemission determination of the Schottky barrier height of metal contacts to n–GaN and p–GaN. *J. Appl. Phys.* **2002**, *92*, 6671–6678, doi:10.1063/1.1518129.
29. Grodzicki, M.; Mazur, P.; Zuber, S.; Perš, J.; Brona, J.; Ciszewski, A. Effect of annealing on Ni/GaN(0001) contact morphology. *Appl. Surf. Sci.* **2014**, *304*, 24–28, doi:10.1016/j.apsusc.2014.01.023.
30. Grodzicki, M.; Mazur, P.; Sabik, A. Impact of surface photovoltage on photoemission from Ni/p-GaN, Applied Surface Science. **2020**, *512*, 145643, doi:10.1016/j.apsusc.2020.145643.

31. Greco, G.; Iucolano, F.; Roccaforte, F. Ohmic contacts to Gallium Nitride materials. *Appl. Surf. Sci.* **2016**, *383*, 324–345, doi:10.1016/j.apsusc.2016.04.016.
32. Wang, W.; Xie, W.; Deng, Z.; Yang, H.; Liao, M.; Li, J.; Luo, X.; Sun, S.; Zhao, D. Performance Improvement of GaN Based Laser Diode Using Pd/Ni/Au Metallization Ohmic Contact. *Coatings* **2019**, *9*, 291, doi:10.3390/coatings9050291.
33. Li, M.; Li, C.; Wang, F.; Zhang, W. The thermodynamic analysis of the driving force for the Ni/GaN interfacial reaction. *Mater. Sci. Eng. A* **2006**, *422*, 316–320, doi:10.1016/j.msea.2006.02.017.
34. Grodzicki, M.; Mazur, P.; Perš, J.; Brona, J.; Zuber, S.; Ciszewski, A. Formation of GaPd2 and GaPd intermetallic compounds on GaN(0001). *Appl. Phys. A* **2015**, *120*, 1443–1451, doi:10.1007/s00339-015-9331-9.
35. Sharafutdinov, I.; Elkjær, C.F.; De Carvalho, H.W.P.; Gardini, D.; Chiarello, G.L.; Damsgaard, C.D.; Wagner, J.B.; Grunwaldt, J.-D.; Dahl, S.; Chorkendorff, I. Intermetallic compounds of Ni and Ga as catalysts for the synthesis of methanol. *J. Catal.* **2014**, *320*, 77–88, doi:10.1016/j.jcat.2014.09.025.
36. Studt, F.; Sharafutdinov, I.; Abild-Pedersen, F.; Elkjær, C.F.; Hummelshøj, J.S.; Dahl, S.; Chorkendorff, I.; Nørskov, J.K. Discovery of a Ni-Ga catalyst for carbon dioxide reduction to methanol. *Nat. Chem.* **2014**, *6*, 320–324, doi:10.1038/nchem.1873.
37. Kovnir, K.; Armbrüster, M.; Teschner, D.; Venkov, T.; Jentoft, F.; Knop-Gericke, A.; Grin, Y.; Schlögl, R. A new approach to well-defined, stable and site-isolated catalysts. *Sci. Technol. Adv. Mater.* **2007**, *8*, 420–427, doi:10.1016/j.stam.2007.05.004.
38. Osswald, J.; Giedigkeit, R.; Jentoft, R.; Armbrüster, M.; Girgsdies, F.; Kovnir, K.; Ressler, T.; Grin, Y.; Schlögl, R. Palladium–gallium intermetallic compounds for the selective hydrogenation of acetylenePart I: Preparation and structural investigation under reaction conditions. *J. Catal.* **2008**, *258*, 210–218, doi:10.1016/j.jcat.2008.06.013.
39. Osswald, J.; Kovnir, K.; Armbrüster, M.; Giedigkeit, R.; Jentoft, R.E.; Wild, U.; Grin, Y.; Schlögl, R. Palladium–gallium intermetallic compounds for the selective hydrogenation of acetylenePart II: Surface characterization and catalytic performance. *J. Catal.* **2008**, *258*, 219–227, doi:10.1016/j.jcat.2008.06.014.
40. Kovnir, K.; Armbrüster, M.; Teschner, D.; Venkov, T.; Szentmiklósi, L.; Jentoft, F.; Knop-Gericke, A.; Grin, Y.; Schlögl, R. In situ surface characterization of the intermetallic compound PdGa–A highly selective hydrogenation catalyst. *Surf. Sci.* **2009**, *603*, 1784–1792, doi:10.1016/j.susc.2008.09.058.
41. Armbrüster, M.; Schlögl, R.; Grin, Y. Intermetallic compounds in heterogeneous catalysis—A quickly developing field. *Sci. Technol. Adv. Mater.* **2014**, *15*, 34803, doi:10.1088/1468-6996/15/3/034803.
42. Foxon, C.; Cheng, T.; Novikov, S.; Jeffs, N.; Hughes, O.; Melnik, Y.; E Nikolaev, A.; Dmitriev, V. Gallium-induced surface reconstruction patterns of GaN grown by molecular beam epitaxy. *Surf. Sci.* **1999**, *421*, 377–385, doi:10.1016/s0039-6028(98)00867-x.
43. Hughes, O.; Cheng, T.; Novikov, S.; Foxon, C.; Korakakis, D.; Jeffs, N. RHEED studies of the GaN surface during growth by molecular beam epitaxy. *J. Cryst. Growth* **1999**, *201*, 388–391, doi:10.1016/s0022-0248(98)01354-2.
44. Ramachandran, V.; Lee, C.; Feenstra, R.M.; Smith, A.; Northrup, J.; Greve, D. Structure of clean and arsenic-covered GaN(0001) surfaces. *J. Cryst. Growth* **2000**, *209*, 355–363, doi:10.1016/s0022-0248(99)00570-9.
45. Vézian, S.; Semond, F.; Massies, J.; Bullock, D.; Ding, Z.; Thibado, P. Origins of GaN(0001) surface reconstructions. *Surf. Sci.* **2003**, *541*, 242–251, doi:10.1016/s0039-6028(03)00950-6.
46. Pei, C.W.; Turk, B.; Héroux, J.B.; Wang, W.I. GaN grown by molecular beam epitaxy with antimony as surfactant. *J. Vac. Sci. Technol. B: Microelectron. Nanometer Struct.* **2001**, *19*, 1426, doi:10.1116/1.1374627.
47. Gokhale, A.A.; Kuech, T.F.; Mavrikakis, M. Surfactant effect of Sb on GaN growth. *J. Cryst. Growth* **2005**, *285*, 146–155, doi:10.1016/j.jcrysgro.2005.08.021.
48. Shan, W.; Ager, J.W.; Yu, K.; Walukiewicz, W.; Haller, E.E.; Martín, M.C.; McKinney, W.R.; Yang, W. Dependence of the fundamental band gap of AlxGa1−xN on alloy composition and pressure. *J. Appl. Phys.* **1999**, *85*, 8505–8507, doi:10.1063/1.370696.
49. Wu, J.; Walukiewicz, W.; Yu, K.M.; Denlinger, J.D.; Shan, W.; Ager, J.W.; Kimura, A.; Tang, H.F.; Kuech, T.F. Valence band hybridization in N-rich GaN(1-x)As(x) alloys. *Phys. Rev. B.* **2004**, *70*, 115214, doi:10.1103/PhysRevB.70.115214.
50. Zdanowicz, E.; Ciechanowicz, P.; Opołczyńska, K.; Majchrzak, D.; Rousset, J.-G.; Piskorska-Hommel, E.; Grodzicki, M.; Komorowska, K.; Serafinczuk, J.; Hommel, D.; et al. As-related stability of the band gap temperature dependence in N-rich GaNAs. *Appl. Phys. Lett.* **2019**, *115*, 092106, doi:10.1063/1.5110245.

51. Grodzicki, M.; Rousset, J.-G.; Ciechanowicz, P.; Piskorska-Hommel, E.; Hommel, D. XPS studies on the role of arsenic incorporated into GaN. *VAC* **2019**, *167*, 73–76, doi:10.1016/j.vacuum.2019.05.043.
52. Yu, K.; Sarney, W.L.; Novikov, S.; Detert, D.; Zhao, R.; Denlinger, J.D.; Svensson, S.; Dubon, O.D.; Walukiewicz, W.; Foxon, C. Highly mismatched N-rich GaN1−xSbx films grown by low temperature molecular beam epitaxy. *Appl. Phys. Lett.* **2013**, *102*, 102104, doi:10.1063/1.4795446.
53. Yu, K.; Novikov, S.; Ting, M.; Sarney, W.L.; Svensson, S.; Shaw, M.; Martin, R.W.; Walukiewicz, W.; Foxon, C. Growth and characterization of highly mismatched GaN1−xSbx alloys. *J. Appl. Phys.* **2014**, *116*, 123704, doi:10.1063/1.4896364.
54. Segercrantz, N.; Yu, K.; Ting, M.; Sarney, W.L.; Svensson, S.; Novikov, S.; Foxon, C.; Walukiewicz, W. Electronic band structure of highly mismatched GaN1−xSbx alloys in a broad composition range. *Appl. Phys. Lett.* **2015**, *107*, 142104, doi:10.1063/1.4932592.
55. Thao, C.P.; Tuan, T.T.A.; Kuo, D.-H.; Ke, W.-C.; Na Thach, T.V.S.; Cao, P.T. Reactively Sputtered Sb-GaN Films and its Hetero-Junction Diode: The Exploration of the n-to-p Transition. *Coatings* **2020**, *10*, 210, doi:10.3390/coatings10030210.
56. Segercrantz, N.; Baumgartner, Y.; Ting, M.; Yu, K.; Mao, S.S.; Sarney, W.L.; Svensson, S.; Walukiewicz, W. Undoped p-type GaN1−xSbx alloys: Effects of annealing. *Appl. Phys. Lett.* **2016**, *109*, 252102, doi:10.1063/1.4972559.
57. Grodzicki, M.; Rousset, J.-G.; Ciechanowicz, P.; Piskorska-Hommel, E.; Hommel, D. Surface studies of physicochemical properties of As films on GaN(0001). *Appl. Surf. Sci.* **2019**, *493*, 384–388, doi:10.1016/j.apsusc.2019.07.006.
58. Grodzicki, M.; Mazur, P.; Pers, J.; Zuber, S.; Ciszewski, A. Sb Layers on p-GaN: UPS, XPS and LEED Study. *Acta Phys. Pol. A* **2014**, *126*, 1128–1130, doi:10.12693/aphyspola.126.1128.
59. Feenstra, R.M.; Northrup, J.E.; Neugebauer, J. Review of Structure of Bare and Adsorbate-Covered GaN(0001) Surfaces. *MRS Internet J. Nitride Semicond. Res.* **2002**, *7*, doi:10.1557/S1092578300000296.
60. Eller, B.S.; Yang, J.; Nemanich, R.J. Electronic surface and dielectric interface states on GaN and AlGaN. *J. Vac. Sci. Technol. A* **2013**, *31*, 050807, doi:10.1116/1.4807904.
61. Bermudez, V. The fundamental surface science of wurtzite gallium nitride. *Surf. Sci. Rep.* **2017**, *72*, 147–315, doi:10.1016/j.surfrep.2017.05.001.
62. Majchrzak, D.; Grodzicki, M.; Ciechanowicz, P.; Rousset, J.; Piskorska-Hommel, E.; Hommel, D. The Influence of Oxygen and Carbon Contaminants on the Valence Band of p-GaN(0001). *Acta Phys. Pol. A* **2019**, *136*, 585–588, doi:10.12693/aphyspola.136.585.
63. Long, J.P.; Bermudez, V.M. Band bending and photoemission-induced surface photovoltages on clean n—And p -GaN (0001) surfaces. *Phys. Rev. B* **2002**, *66*, 121308, doi:10.1103/physrevb.66.121308.
64. Grodzicki, M.; Moszak, K.; Hommel, D.; Bell, G.R. Band alignment and surface Fermi level pinning in GaN. *Appl. Surf. Sci.* under review.
65. Pugh, S.; Dugdale, D.; Brand, S.; Abram, R. Electronic Structure Calculations on Nitride Semiconductors. *Semicond. Sci. Technol.* **1999**, *14*, 23, doi:10.1088/0268-1242/14/1/003.
66. *Semiconductors*; Springer Science and Business Media LLC: Berlin/Heidelberg, Germany, 1991.
67. Madelung, O.; Madelung, O. *Semiconductors: Data Handbook*; Springer: Berlin, Germany, 2004.
68. Levinshtein, M.E.; Rumyantsev, S.L.; Shur, M.S. Properties of Advanced Semiconductor Materials: GaN, AIN, InN, BN, SiC, SiGe | Wiley, 2001. Available online: https://www.wiley.com/en-us/Properties+of+Advanced+Semiconductor+Materials%3A+GaN%2C+AIN%2C+InN%2C+BN%2C+SiC%2C+SiGe-p-9780471358275 (accessed on 28 April 2020).
69. Falta, J.; Schmidt, T.; Gangopadhyay, S.; Schulz, C.; Kuhr, S.; Berner, N.; Flege, J.I.; Pretorius, A.; Rosenauer, A.; Sebald, K.; et al. Cleaning and growth morphology of GaN and InGaN surfaces. *Phys. Status Solidi (b)* **2011**, *248*, 1800–1809, doi:10.1002/pssb.201046574.
70. Kova, J.; Zalar, A.; Kovač, J. Surface composition changes in GaN induced by argon ion bombardment. *Surf. Interface Anal.* **2002**, *34*, 253–256, doi:10.1002/sia.1294.
71. Despiau-Pujo, E.; Chabert, P. MD simulations of GaN sputtering by Ar[sup +] ions: Ion-induced damage and near-surface modification under continuous bombardment. *J. Vac. Sci. Technol. A* **2010**, *28*, 1105, doi:10.1116/1.3460904.
72. Hunt, R.; Vanzetti, L.; Castro, T.; Chen, K.; Sorba, L.; Cohen, P.; Gladfelter, W.; Van Hove, J.; Kuznia, J.; Khan, M.; et al. Electronic structure, surface composition and long-range order in GaN. *Phys. B Condens. Matter* **1993**, *185*, 415–421, doi:10.1016/0921-4526(93)90271-7.

73. Grodzicki, M.; Mazur, P.; Ciszewski, A. Modification of Electronic Structure of n-GaN(0001) Surface by N + -Ion Bombardment. *Acta Phys. Pol. A* **2017**, *132*, 351–353, doi:10.12693/APhysPolA.132.351.
74. Grodzicki, M.; Mazur, P.; Ciszewski, A. Changes of electronic properties of p-GaN(0 0 0 1) surface after low-energy N+-ion bombardment. *Appl. Surf. Sci.* **2018**, *440*, 547–552, doi:10.1016/j.apsusc.2018.01.097.
75. Koleske, D.; Wickenden, A.E.; Henry, R.; DeSisto, W.J.; Gorman, R.J. Growth model for GaN with comparison to structural, optical, and electrical properties. *J. Appl. Phys.* **1998**, *84*, 1998–2010, doi:10.1063/1.368353.
76. Janzen, O.; Hahn, C.; Kampen, T.; Mönch, W. Explanation of multiplet spots in low-energy electron diffraction patterns of clean GaN surfaces. *Eur. Phys. J. B* **1999**, *7*, 1–4, doi:10.1007/s100510050583.
77. Tautz, F.; Sloboshanin, S.; Starke, U.; Schaefer, J. Reactivity and morphology of-faceted and (3 × 3)-reconstructed gan (000) epilayers grown on sapphire (0001). *J. Phys. Condens. Matter* **1999**, *11*, 8035.
78. Segev, D.; Van De Walle, C.G. Origins of Fermi-level pinning on GaN and InN polar and nonpolar surfaces. *EPL (Europhysics Lett.* **2006**, *76*, 305–311, doi:10.1209/epl/i2006-10250-2.
79. Van De Walle, C.G.; Segev, D. Microscopic origins of surface states on nitride surfaces. *J. Appl. Phys.* **2007**, *101*, 081704, doi:10.1063/1.2722731.
80. Janicki, Ł.; Gładysiewicz, M.; Misiewicz, J.; Klosek, K.; Sobanska, M.; Kempisty, P.; Zytkiewicz, Z.R.; Kudrawiec, R. Contactless electroreflectance studies of the Fermi level position at the air/GaN interface: Bistable nature of the Ga-polar surface. *Appl. Surf. Sci.* **2017**, *396*, 1657–1666, doi:10.1016/j.apsusc.2016.12.013.
81. Shi, M.; Chinchore, A.; Wang, K.; Mandru, A.-O.; Liu, Y.; Smith, A.R. Formation of manganese δ-doped atomic layer in wurtzite GaN. *J. Appl. Phys.* **2012**, *112*, 53517, doi:10.1063/1.4750034.
82. Chinchore, A.; Wang, K.; Lin, W.; Pak, J.; Smith, A.R. Atomic layer structure of manganese atoms on wurtzite gallium nitride (000 1). *Appl. Phys. Lett.* **2008**, *93*, 181908.
83. Chinchore, A.V.; Wang, K.; Shi, M.; Mandru, A.; Liu, Y.; Haider, M.; Smith, A.R.; Ferrari, V.; Barral, M.A.; Ordejon, P. Manganese 3 × 3 and 3 × 3—R30° structures and structural phase transition on w -GaN(000 1¯) studied by scanning tunneling microscopy and first-principles theory. *Phys. Rev. B* **2013**, *87*, 165426, doi:10.1103/physrevb.87.165426.
84. Waldrop, J.R.; Grant, R.W.; Wang, Y.C.; Davis, R.F. Metal Schottky barrier contacts to alpha 6H-SiC. *J. Appl. Phys.* **1992**, *72*, 4757–4760, doi:10.1063/1.352086.
85. Waldrop, J.R. Schottky barrier height of metal contacts to p-type alpha 6H-SiC. *J. Appl. Phys.* **1994**, *75*, 4548–4550, doi:10.1063/1.355948.
86. Reed, M.; Ritums, M.; Stadelmaier, H.; Reed, M.; Parker, C.; Bedair, S.; El-Masry, N. Room temperature magnetic (Ga,Mn)N: A new material for spin electronic devices. *Mater. Lett.* **2001**, *51*, 500–503, doi:10.1016/s0167-577x(01)00342-1.
87. Reed, M.L.; El-Masry, N.A.; Stadelmaier, H.H.; Ritums, M.K.; Reed, M.J.; Parker, C.A.; Roberts, J.C.; Bedair, S.M. Room temperature ferromagnetic properties of (Ga, Mn)N. *Appl. Phys. Lett.* **2001**, *79*, 3473–3475, doi:10.1063/1.1419231.
88. Hobbs, D.; Hafner, J.; Spišák, D. Understanding the complex metallic element Mn. I. Crystalline and noncollinear magnetic structure of $\alpha$-Mn. *Phys. Rev. B* **2003**, *68*, doi:10.1103/physrevb.68.014407.
89. Lu, Q.M.; Yue, M.; Zhang, H.G.; Wang, M.L.; Yu, F.; Huang, Q.Z.; Ryan, D.H.; Altounian, Z. Intrinsic magnetic properties of single-phase Mn1+xGa (0 < x < 1) alloys. *Sci. Rep.* **2015**, *5*, 17086, doi:10.1038/srep17086.
90. Arins, A.; Jurca, H.; Zarpellon, J.; Fabrim, Z.; Fichtner, P.F.P.; Varalda, J.; Schreiner, W.; Mosca, D. Correlation between tetragonal zinc-blende structure and magnetocrystalline anisotropy of MnGa epilayers on GaAs(111). *J. Magn. Magn. Mater.* **2015**, *381*, 83–88, doi:10.1016/j.jmmm.2014.12.068.
91. Hwang, J.I.; Ishida, Y.; Kobayashi, M.; Hirata, H.; Takubo, K.; Mizokawa, T.; Fujimori, A.; Okamoto, J.; Mamiya, K.; Saito, Y.; et al. High-energy spectroscopic study of the III-V nitride-based diluted magnetic semiconductorGa1−xMnxN. *Phys. Rev. B* **2005**, *72*, 085216, doi:10.1103/physrevb.72.085216.
92. Brudnyi, V.N. Gallium Nitride: Charge Neutrality Level and Interfaces. *Russ. Phys. J.* **2016**, *58*, 1613–1618, doi:10.1007/s11182-016-0691-1.
93. Majid, A.; Ahmad, N.; Rizwan, M.; Khan, S.U.-D.; Ali, F.A.A.; Zhu, J. Effects of Mn Ion Implantation on XPS Spectroscopy of GaN Thin Films. *J. Electron. Mater.* **2017**, *47*, 1555–1559, doi:10.1007/s11664-017-5955-1.

94. Kulatov, E.; Nakayama, H.; Mariette, H.; Ohta, H.; Uspenskii, Y.A. Electronic structure, magnetic ordering, and optical properties of GaN and GaAs doped with Mn. *Phys. Rev. B* **2002**, *66*, 045203, doi:10.1103/physrevb.66.045203.
95. Barthel, S.; Kunert, G.; Gartner, M.; Stoica, M.; Mourad, D.; Kruse, C.; Figge, S.; Hommel, D.; Czycholl, G. Determination of the Fermi level position in dilute magnetic Ga1-xMnxN films. *J. Appl. Phys.* **2014**, *115*, 123706, doi:10.1063/1.4869134.
96. Titov, A.; Biquard, X.; Halley, D.; Kuroda, S.; Bellet-Amalric, E.; Mariette, H.; Cibert, J.; Merad, A.E.; Merad, G.; Kanoun, M.-B.; et al. X-ray absorption near-edge structure and valence state of Mn in (Ga,Mn)N. *Phys. Rev. B* **2005**, *72*, 115209, doi:10.1103/physrevb.72.115209.
97. Nörenberg, C.; Myhra, S.; Dobson, P.J. Scanning probe microscopy studies on the growth of palladium and nickel on GaN(0001). *J. Physics: Conf. Ser.* **2010**, *209*, 012021, doi:10.1088/1742-6596/209/1/012021.
98. Pers, J.; Grodzicki, M.; Ciszewski, A. Topography of thin films containing Ni-Ga intermetallic compounds formed on GaN(0001). *Copernic. Lett.* **2016**, *7*, 1, doi:10.12775/CL.2016.001.
99. Maruyama, T.; Hagio, Y.; Miyajima, T.; Kijima, S.; Nanishi, Y.; Akimoto, K. Effects of annealing on the interface properties between ni and p-gan. *Phys. Status Solidi (A)* **2001**, *188*, 375–378.
100. Barinov, A.; Gregoratti, L.; Kaulich, B.; Kiskinova, M.; Rizzi, A. Defect-induced lateral chemical heterogeneity at Ni/GaN interfaces and its effect on the electronic properties of the interface. *Appl. Phys. Lett.* **2001**, *79*, 2752–2754, doi:10.1063/1.1404411.
101. Grodzicki, M.; Mazur, P.; Zuber, S.; Pers, J.; Ciszewski, A. Pd/GaN(0001) interface properties. *Mater. Sci.* **2014**, *32*, 252–256, doi:10.2478/s13536-013-0183-8.
102. Hsu, L.-S.; Williams, R.S. Electronic-structure study of the Ni Ga and the Ni In intermetallic compounds using X-ray photoemission spectroscopy. *J. Phys. Chem. Solids* **1994**, *55*, 305–312, doi:10.1016/0022-3697(94)90226-7.
103. Hsu, L.-S.; Gweon, G.-H.; Allen, J. Electronic-structure study of Ni3Al, Ni3Ga, Ni3In, and NiGa using X-ray photoemission spectroscopy and Bremsstrahlung isochromat spectroscopy. *J. Phys. Chem. Solids* **1999**, *60*, 1627–1631, doi:10.1016/s0022-3697(99)00196-1.
104. Alonso, M.; Cimino, R.; Horn, K. Surface photovoltage effects in photoemission from metal-GaP(110) interfaces: Importance for band bending evaluation. *Phys. Rev. Lett.* **1990**, *64*, 1947–1950, doi:10.1103/physrevlett.64.1947.
105. Cossu, G.; Ingo, G.M.; Mattogno, G.; Padeletti, G.; Proietti, G. XPS investigation on vacuum thermal desorption of UV/ozone treated GaAs(100) surfaces. *Appl. Surf. Sci.* **1992**, *56*, 81–88, doi:10.1016/0169-4332(92)90219-n.
106. Kraut, E.A.; Grant, R.W.; Waldrop, J.R.; Kowalczyk, S.P. Precise Determination of the Valence-Band Edge in X-Ray Photoemission Spectra: Application to Measurement of Semiconductor Interface Potentials. *Phys. Rev. Lett.* **1980**, *44*, 1620–1623, doi:10.1103/PhysRevLett.44.1620.
107. Arabasz, S.; Bergignat, E.; Hollinger, G.; Szuber, J. XPS analysis of surface chemistry of near surface region of epiready GaAs(100) surface treated with (NH4)2Sx solution. *Appl. Surf. Sci.* **2006**, *252*, 7659–7663, doi:10.1016/j.apsusc.2006.03.061.
108. Grodzicki, M.; Mazur, P.; Wasielewski, R.; Ciszewski, A. Physicochemical properties of the Sb/p-SiC interface. *VAC* **2017**, *146*, 216–220, doi:10.1016/j.vacuum.2017.09.037.
109. Wang, M.W. Study of interface asymmetry in InAs–GaSb heterojunctions. *J. Vac. Sci. Technol. B Microelectron. Nanometer Struct.* **1995**, *13*, 1689, doi:10.1116/1.587879.


© 2020 by the authors. Licensee MDPI, Basel, Switzerland. This article is an open access article distributed under the terms and conditions of the Creative Commons Attribution (CC BY) license (http://creativecommons.org/licenses/by/4.0/).